Soil Dynamics and Earthquake Engineering 183 (2024) 108758

Contents lists available at ScienceDirect

Soil Dynamics and Earthquake Engineering

journal homepage: www.elsevier.com/locate/soildyn

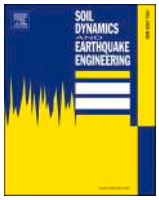

Approximate decoupling of topographic, stratigraphic and valley effects on the peak seismic acceleration

Annamaria di Lernia [a,*], Achilleas G. Papadimitriou [b], Gaetano Elia [a]

[a] Department of Civil, Environmental, Land, Building Engineering and Chemistry (DICATECh), Technical University of Bari, via Orabona 4, 70125, Bari, Italy
[b] School of Civil Engineering, National Technical University of Athens, 9 Iroon Polytechniou Str., 15780, Zographou, Greece

ARTICLE INFO

Keywords:
Seismic site effects
Topographic effects
Stratigraphic effects
Valley effects
FE modelling
Analytical formulations
Site amplification

ABSTRACT

The seismic amplification of any given area is a combined result of topographic, stratigraphic and valley effects. Nevertheless, quantifying the contribution of each of these three effects in the overall amplification is not straightforward. To this end, this paper proposes a procedure for the approximate decoupling of these effects on the amplification of the peak seismic acceleration at the ground surface. This is performed by setting the pertinent site amplification factor equal to the product of three spatially-variable amplification factors, one for each of these effects. The procedure employs two-dimensional (2D) linear visco-elastic numerical simulations and simplified analytical formulations, the latter aiming at the quantification of the one-dimensional (1D) amplification of soil-bedrock and (solely) bedrock columns. As an example, the decoupling procedure is applied to a slope with irregular topography, characterised by a homogeneous soil layer overlying bedrock. The ground response analyses employ Ricker wavelet excitations, characterised by different predominant periods covering the range of periods related to typical earthquakes, as well as actual seismic recordings. The results depict that the three amplification factors depend on the seismic excitation and vary widely along the study area (taking values that range from 0.6 up to 1.7). The proposed procedure is an approximate, but reliable tool for decoupling the spatially-variable contributions of the aforementioned effects, at least when the visco-elastic conditions are realistic. As such, it may be used as an expeditive tool for identifying regions mostly affected by each of these effects, thus guiding the need for additional site investigation or in-depth analysis.

1. Introduction

Numerous destructive earthquake events in the past have already underlined the crucial role of local site conditions on the propagation of the seismic motion reaching the ground surface of an area [1–9]. Indeed, site conditions, i.e. the surface topography, the soil stratigraphy and the buried bedrock morphology, can increase (or sometimes decrease) the intensity of the seismic motion and modify its duration and its frequency content. The overall modification of the seismic motion reaching the ground surface is collectively referred to with the term “site effects”. These effects vary per location at the ground surface, since they arise as a combination of “topographic effects”, “stratigraphic effects” and “valley effects”. Specifically, the term “topographic effects” refers to the seismic motion alteration related to the shape and inclination of the surface topography, while the one-dimensional (1D) “stratigraphic effects” are related to the filtering processes of the seismic waves propagating through a sequence of horizontal soil layers over horizontal bedrock, all characterised by different dynamic properties in terms of stiffness and dissipative capacity. Finally, “valley effects” refer to the seismic motion modification due to the inclination of interfaces between successive soil layers and between the soil and the bedrock, including the formation of closed soil basins over laterally outcropping bedrock. In some of the published literature, any seismic motion alteration that is not due to “stratigraphic effects” is collectively attributed to “topographic effects”, but in this paper the foregoing clear distinction is made, which attributes to “topographic effects” only the modification due to surface topography.

Each of these effects, or a combination thereof, may be responsible for disastrous consequences during an earthquake. For example, topographic effects were deemed to be the main responsible for the severe damages observed during many devastating earthquakes, such as the 1985 Canal Beagle Chile earthquake [10,11], the 1987 Whittier Narrows California earthquake [12], the 1995 Aegion Greece earthquake [3,13], the 1999 Athens Greece earthquake [5], the Haiti 2010 earthquake [14],

* Corresponding author.
E-mail addresses: annamaria.dilernia@poliba.it (A. di Lernia), apapad@civil.ntua.gr (A.G. Papadimitriou), gaetano.elia@poliba.it (G. Elia).

https://doi.org/10.1016/j.soildyn.2024.108758
Received 26 February 2024; Received in revised form 20 May 2024; Accepted 31 May 2024

the 2016 Central Italy earthquake [15,16]. Similarly, stratigraphic effects were considered the culprit for the extensive damages to structures and infrastructures and the numerous loss of lives in Mexico City during the famous 1985 Mexico earthquake [17]. Most often, the morphology of the stratigraphic contacts add to the effect of the subsoil succession, exacerbating the seismic amplifications as in the case of the 1988 Armenia earthquake [18,19], the 1989 Loma Prieta earthquake [20], the 2002 Molise earthquake [21], the 2012 Emilia Romagna earthquake [22], or the recent 2020 Samos earthquake [23], where valley effects have been pinpointed as responsible for the observed disaster.

In addition to the severe damages to buildings and infrastructures caused by the amplification of the seismic motion, the site effects may also trigger either the onset or the reactivation of landslides [24], as in the case of the 1994 Northridge earthquake [25], the 2008 Wenchuan earthquake [26,27], the 2010 Haiti earthquake [28], the 2016 Central Italy earthquake [29], to cite few. Therefore, the estimation of site effects represents a crucial issue in the assessment and the management of the seismic risk, especially in the case of old towns located on hilltops characterised by urban aggregates of masonry buildings or within areas prone to landsliding [30–37].

From a practical point of view, decoupling the contributions of these effects in the seismic amplification of any given site may be quite useful. Firstly, it allows the identification of areas where each of these three effects may be either more pronounced or irrelevant and, this may act as a guide for depicting the areas requiring additional site investigation or in-depth analyses. Secondly, the separate quantification of these effects provides insights into the complex phenomena of the seismic wave propagation, but more importantly it may pave the way for a safer structural design, since it is aligned with the simplified manner by which seismic codes also attempt to quantify site effects. For example, topographic effects are incorporated in the Eurocode 8 (EC8) provisions as a multiplier of the whole design spectrum selected on the basis of the soil stratigraphy. This methodology has prompted many researchers to address these effects in a similar simplified manner [38].

Unfortunately, this decoupling of site effects is not always easy or possible to be performed, except for cases where only one of these effects appears, i.e., horizontal soil layers over a horizontal bedrock under vertically impinging S waves, where the observed site effects are only due to stratigraphic effects. To make matters worse, in many literature studies the reference locations for quantifying these effects are not the same, thus making difficult to compare results and extract common conclusions. For example, in the seminal studies of Bard and Bouchon [39–41] the amplification of the peak ground acceleration of two-dimensional (2D) alluvial valleys with a horizontal ground surface is measured in comparison to the free-field bedrock response. Hence, the estimated amplification is a combination of stratigraphic and valley effects. On the other hand, for similar 2D valley geometries, many studies [8,42–45] decouple valley from stratigraphic effects, by dividing the amplification along the valley surface with the one-dimensional (1D) stratigraphic amplification factor, which is correct along the central section of the valley, but only approximate above its inclined bedrock edges (where the soil has a different thickness at each location). Similarly, valley effects have been estimated for alluvial basins, by comparing results of 2D nonlinear time-domain analyses with 1D nonlinear simulation in terms of the spectral aggravation factor, defined as the ratio between 2D and 1D acceleration response spectra for each period. It was shown that the inclination of the bedrock may strongly influence the seismic response of the basin [46–48]. Likewise, for the estimation of topographic effects in homogeneous hills or canyons, it is customary to consider the free-field as the reference location [49–52]. However, in step-like homogeneous slopes, the reference locations behind the crest and in front of the toe are at different elevations. Hence, Bouckovalas and Papadimitriou [53] estimated the amplification values along the horizontal ground surface in comparison to their respective free-field response values, something that cannot be performed accurately along the inclined slope (each point of which is at a different elevation). When there is a "soft soil" layer behind the crest (e.g. Refs. [5,13]) or a soil-bedrock interface below the elevation of the toe (e.g., Ref. [54]), the foregoing free-field amplification values include also 1D stratigraphic effects, which are also different along the inclined slope making their decoupling a complicated task.

Based on the above, it becomes obvious that the decoupling of topographic, stratigraphic and valley effects on seismic ground motion is useful, but far from straightforward. As explained above, the problem lies on the fact that these effects have not been univocally defined in the literature, but also because the published studies usually focus on a select subset of these effects (depending on the case history or the employed methodology). To this end, the paper presents an approximate procedure for decoupling the components of 2D site effects on the amplification of the peak horizontal seismic acceleration at the ground surface. The proposed procedure employs 2D (and limited number of 1D) visco-elastic numerical simulations, as well as the use of analytical formulations for the prediction of the 1D amplification at the ground surface. The procedure is presented herein with reference to an example slope, but it is applicable for any ground surface and soil-bedrock interface geometry. Its applicability is limited (so far) to cases of excitations with low and intermediate intensity, for which the visco-elastic approximation is realistic. To the authors' knowledge, there are no works in the literature that have proposed any similar procedure for concurrently decoupling these three effects on site amplification for any generic study area. Hence, despite its limitations, the proposed methodology is considered a novel and expeditive tool for the task at hand.

2. A strategy for decoupling the amplification factors

Fig. 1 presents a general scheme of a 2D homogeneous linear visco-elastic soil layer over homogeneous seismic bedrock, in which the ground surface is irregular and the soil-bedrock interface form a closed basin. The soil and bedrock materials are characterised by constant values of shear wave velocities equal to V_S and V_R, respectively. The bedrock is defined as the stratum characterised by a shear wave velocity systematically greater than 800 m/s; thus, it is not necessarily a rock material, but it could also be a very stiff soil characterised by high values of the shear wave velocity. In seismic wave propagation processes, the vertically propagating seismic motion may arrive at the ground surface of a soil deposit modified in terms of amplitude, duration and frequency content. In this paper, the emphasis will be put solely on the peak horizontal acceleration and not on the rest of the horizontal acceleration time-history or on any other type of seismic motion characteristic, since this comprises a first attempt of proposing a methodology for decoupling the components of site effects. Moreover, it has been repeatedly demonstrated that the short-period components of the motion (and the peak horizontal acceleration) are generally affected by all three components of site effects. Conversely, large-period components are definitely influenced by stratigraphic effects, but may not be affected so much by topographic or valley effects [38,42]. For the scheme in Fig. 1, the a_0 is the maximum horizontal acceleration for horizontal bedrock conditions (i.e., when there are no site effects of any kind), which is the value usually given by a seismic risk assessment study for rock outcropping conditions. For brevity, this site-specific a_0 value will be referred to hereafter as the input maximum acceleration. In the figure, a^S_{2D} is the spatially-variable maximum horizontal acceleration where the soil outcrops, a^R_{2D} is the spatially-variable maximum horizontal acceleration where the bedrock outcrops. All these maximum horizontal acceleration values have a subscript 2D to underline their spatial variability given 2D wave propagation reflections and refractions.

Hence, the total amplification factor (for the maximum horizontal acceleration) along the ground surface of a 2D model, $AF_{2D}(x)$, is spatially-variable and, by definition, is given as the ratio of $a^S_{2D}(x)$ over the input maximum acceleration a_0. As shown in Eq. (1), this spatially-variable total amplification factor $AF_{2D}(x)$ may be written as the product

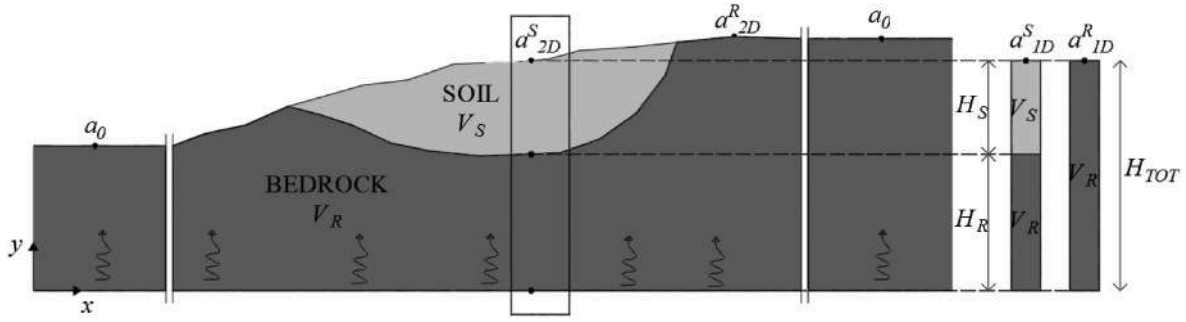

Fig. 1. Schematic illustration of the seismic wave propagation process for a generic soil-bedrock geometry and definition of problem parameters.

of two (2) separate (also spatially-variable) amplification factors, i.e., the (1D) stratigraphic amplification factor AF_{1D} and a combined factor accounting for both topographic and valley effects $A_{TV}(x)$:

$$AF_{2D}(x) = \frac{a^S_{2D}(x)}{a_0} = \frac{a^S_{1D}(x)}{a_0}\frac{a^S_{2D}(x)}{a^S_{1D}(x)} = AF_{1D}(x)\cdot A_{TV}(x) \quad (1)$$

Based on Eq. (1), the (1D) stratigraphic amplification factor AF_{1D} is defined as the ratio of the maximum acceleration at the top of a 1D soil-bedrock column, a^S_{1D}, over the input maximum acceleration, a_0, with this soil-bedrock column having the same total height H_{TOT} of the model at that location x in the 2D analysis. In other words, the AF_{1D} at each location x expresses the amplification that would be observed at that location if both the ground surface and the soil-bedrock interface (if appearing at location x) were horizontal and extended infinitely horizontally, i.e., if 1D conditions prevailed. This amplification factor is typically evaluated through 1D numerical analyses, which can be performed either in the frequency domain or in the time domain [55–62], implementing the sequence and the thickness of the soil layers and the appropriate dynamic properties of the soils. The practical problem for the calculation of factor AF_{1D} is that the a^S_{1D} is spatially-variable, since the heights H_S, H_R and H_{TOT} (=$H_S + H_R$) differ per location (see Fig. 1). This implies the need for a large number of 1D seismic ground response analyses to cover the whole study area. The other multiplier $A_{TV}(x)$ of Eq. (1) may be considered a spatially-variable combined amplification factor due to topographic and valley effects, since the stratigraphic effects have been decoupled via the AF_{1D}. The $A_{TV}(x)$ may be evaluated through the comparison of the 2D site response with the results of the aforementioned numerous 1D simulations. In other words, it may be evaluated as the ratio of a^S_{2D} over the a^S_{1D} value at each location x, as shown in Eq. (1).

If someone considers that "valley effects" are part of "topography effects", then Eq. (1) including the combined amplification factor $A_{TV}(x)$ concludes the decoupling procedure. However, these two effects are considered different in this paper. Hence taking this procedure one step further, the combined amplification factor $A_{TV}(x)$ of Eq. (1) may be written as the product of the Topographic Amplification Factor, $TAF(x)$, and the Valley Amplification Factor, $VAF(x)$, according to Eq. (2):

$$A_{TV}(x) = \frac{a^S_{2D}(x)}{a^S_{1D}(x)} = TAF(x)\cdot VAF(x) \quad (2)$$

The Topographic Amplification Factor $TAF(x)$ expresses what would the topographic amplification be at the study area, if the ground consisted solely of bedrock material. Hence it is a spatially-variable amplification factor that may be estimated according to Eq. (3):

$$TAF(x) = \frac{a^R_{2D}(x)}{a^R_{1D}(x)} \quad (3)$$

where $a^R_{2D}(x)$ is the maximum horizontal acceleration at the ground surface of a fictitious 2D homogeneous ground model with the same topography of the study area, but consisting solely of bedrock material, whereas $a^R_{1D}(x)$ is the maximum horizontal acceleration at the surface of the 1D bedrock column at each location x. These 1D bedrock columns have the same total height H_{TOT} as the 1D soil-bedrock columns at each location x but comprise of solely bedrock material.

By substituting Eq. (3) into Eq. (2) and by solving for the Valley Amplification Factor $VAF(x)$, this is given by:

$$VAF(x) = \frac{a^S_{2D}(x)}{a^R_{2D}(x)}\frac{a^R_{1D}(x)}{a^S_{1D}(x)} \quad (4)$$

Thus, for the estimation of the above-mentioned spatially-variable amplification factors, the proposed procedure requires the numerical execution of two 2D dynamic linear visco-elastic analyses, one with true soil-bedrock layers and a fictitious one with the same topography, but consisting solely of bedrock material. Moreover, it requires the estimation of the 1D stratigraphic effects, through the execution of 1D numerical seismic ground response analyses for the soil-bedrock and the bedrock columns, identified at the location of each observation point at the ground surface of the 2D slope model. This step could be carried out either by performing a large number of 1D ground response analyses (implying high computational costs), or approximately by adopting multi-variable analytical formulations, outlined in the following, whose parameters are appropriately calibrated through the execution of a small number of 1D analyses.

3. Example case and employed numerical methodology

The proposed strategy for decoupling the topographic, stratigraphic and valley effects is illustrated with reference to an example slope, whose topographic profile is based on the real slope described in Ref. [32]. The example slope is characterised by a homogeneous soil layer of shear wave velocity V_S equal to 626 m/s, overlying a bedrock layer with a shear wave velocity V_R equal to 1250 m/s, whose soil-bedrock interface is inclined and sub-parallel to the topography, according to the real slope conditions (Fig. 2a). Thus, based on the literature, relatively unimportant valley effects are expected in this specific area, since the soil-bedrock interface does not form a closed basin (e.g., Refs. [42–44]). On the contrary, topographic effects should appear given the surface topography, with the highest amplification appearing in the proximity of where the steepest surface inclination appears (e.g., Ref. [53]). Finally, stratigraphic effects are expected to be more or less uniform along the area, given the homogeneity and the approximately constant thickness of the soil layer according to 1D wave propagation theory (e.g., Ref. [63]). Hence, besides showcasing the proposed methodology, this example application should also depict whether this decoupling procedure is able to distinguish locations or excitations where each of these three effects becomes important or not.

The required numerical simulations of the seismic wave propagation processes are performed via the 2D finite element (FE) code PLAXIS 2D [64]. The 2D plane-strain FE model, illustrated in Fig. 2a, is characterised by a slope length, L_{slope}, equal to 892 m and a height, H_{slope}, equal to 104 m, with an average inclination of about 9°. The contact between

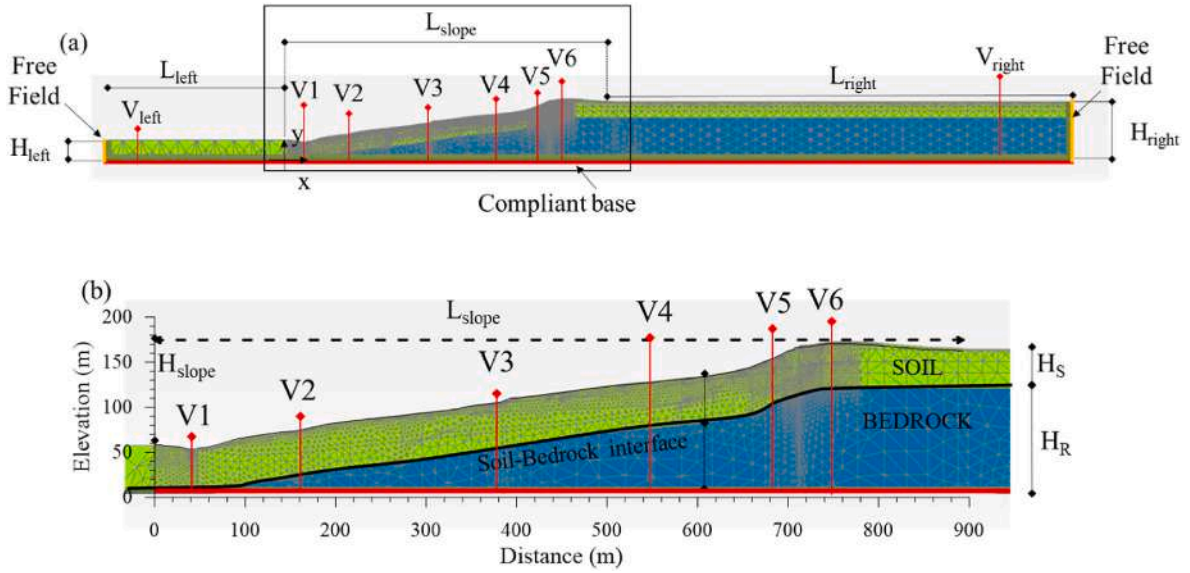

Fig. 2. Numerical model implemented in the FE simulations, definition of geometrical problem parameters and locations of 1D vertical profiles: (a) the whole model, (b) detail of the studied slope.

the soil layer and the bedrock layer is sub-parallel to the topographic profile and placed at about 50 m below ground level (b.g.l.). Thus, the soil has a thickness H_S of about 50 m, while the bedrock layer is characterised by a thickness H_R variable along the slope model in the range between about 3 m on the left-hand side and about 110 m on the right-hand side (Fig. 2b), depending on the position of the soil-bedrock interface.

The geometrical model of the slope has been laterally extended by 8 times the height of the vertical sides, i.e., 500 m and 1240 m on the left and right side respectively, to avoid any interference of the vertical boundaries with the area of interest along the slope [65]. The 2D soil domain of the slope model has been discretized with 9452 15-node triangular elements, distributed such that a greater refinement is obtained approaching the ground surface. To allow for accurate propagation of the seismic waves through the FE mesh, the distance between two nodes of the finite elements should be small relative to the smallest propagated wavelength. For this reason, along the vertical direction, the node distance is set smaller than 1/8 of the smallest significant S - wavelength of the seismic excitation ($\lambda_{S,\min} = V_S/f_{\max}$, where $f_{\max}$ is the maximum significant frequency of the input motion), while nodes on the ground surface are located within the maximum distance of 1/8 of the smallest wavelength of the Rayleigh waves $\lambda_{R,\min}$ ($\cong 0.94 \cdot V_S/f_{\max}$), in order to capture the frequency content of the vertically propagating S-waves and the horizontally propagating Rayleigh waves, respectively [66,67].

The selected input motions, considered as outcropping motions, have the form of Ricker wavelets (Fig. 3a). Specifically, six (6) input motions characterised by central frequency f_c ranging from 1.6 Hz to 10 Hz, have been selected for the definition of the Ricker wavelets, according to Eq. (5):

$$\frac{a(t)}{a_0} = \left(1 - 2\pi^2 f_c^2 t^2\right)\exp\left(-\pi^2 f_c^2 t^2\right) \tag{5}$$

where a_0 is the maximum acceleration of the input motion. The (normalised over a_0) pseudo-spectral acceleration (PSA) response spectra of all wavelet signals are depicted in Fig. 3b and lie within the range covered by the reference elastic response spectrum provided by Eurocode 8 provisions for Ground Type A (bedrock, for magnitudes M > 5.5). Hence, in terms of frequency content the selected input motions cover the range of typical earthquakes occurring in the broader European area. It is underlined here that the excitation W1 corresponds to a rather extremely short-period motion (predominant period $T_p = 0.08$ s), but it is considered here along with excitations W2 – W6, in order to verify the applicability of the proposed procedure even beyond the expected

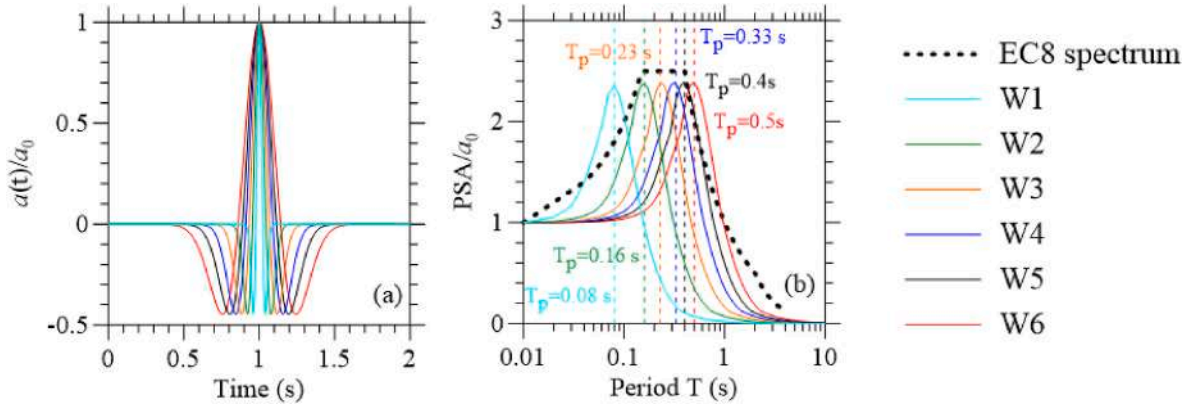

Fig. 3. Characteristics of the selected Ricker wavelets: (a) acceleration time histories and (b) elastic pseudo-spectral acceleration response spectra (for 5 % damping) normalised to the maximum input acceleration a_0 and compared to EC8 design spectrum for bedrock.

Table 1
Characteristics of the selected Ricker wavelets.

Name	f_c (Hz)	T_p (s)
W1	10	0.08
W2	5	0.16
W3	3.33	0.23
W4	2.5	0.33
W5	2	0.4
W6	1.6	0.5

period range (T_p = 0.16–0.50 s) for bedrock motions. The adopted central frequencies f_c of the selected Ricker wavelets and the corresponding predominant periods T_p are summarised in Table 1.

Given the frequency characteristics of the selected input motions and the shear wave velocity of the soil and bedrock layers, with the aim of satisfying the condition on the nodes distance, the mesh has been discretized with reference to the smallest significant S-wavelength among all the examined cases, associated to the lowest-period motion W1 exciting the least stiff material (soil with V_S = 626 m/s). For example, the maximum vertical distance between two nodes in the numerical model is set to be smaller than 3.9 m, aiming to capture the significant frequency content of the lowest-period signal by setting f_{max} = 20 Hz, i.e., a value that is 2 times larger than the largest considered central frequency f_c (=10 Hz for motion W1). The same mesh discretization has been adopted for the totality of the numerical simulations.

The behaviour of the geomaterials is described by the simple linear visco-elastic model, assuming the shear wave velocity constant with depth in each homogeneous layer. For simplicity, all layers are characterised by constant unit weight γ of 19 kN/m^3, Poisson ratio ν equal to 0.25 and at-rest earth pressure coefficient K_0 equal to 0.5. The dissipative capacity of the soil layers has been implemented through the Rayleigh formulation [68], according to Eq. (6):

$$D_{Rayleigh} = \frac{D_{target}}{\frac{1}{T_m}+\frac{1}{T_n}}\left(\frac{2T}{T_m \cdot T_n}+\frac{1}{T}\right) \quad (6)$$

where the control periods T_m and T_n have been selected equal to 1 s and 0.05 s assuming a target damping D_{target} of 7 %. The frequency dependent damping $D_{Rayleigh}$, whose curve is illustrated in Fig. 4 as a function of period T, provide an average damping ratio $D_{average}$ of about 5 %, representative of the dissipative capacity in the 0.001 %–0.01 % strain range [69,70]. The corresponding Rayleigh parameters α_R and β_R, computed through Eq. (7), are equal to 0.8378 and 0.001061, respectively.

$$\alpha_R = \frac{4\pi D_{target}}{T_m + T_n} \quad \beta_R = \frac{D_{target}}{\pi}\frac{T_m \cdot T_n}{T_m + T_n} \quad (7)$$

After the initial stage of stress state generation, the dynamic stage has been carried out by applying different input motions at the bottom of the FE model via the compliant base boundary condition [64]. This entails absorbing boundaries, which simulate the dissipation of the waves into the bedrock half-space with minimum reflection at the bottom of the mesh [71]. In addition, since only the upward propagating motion is considered, only half of the input motion at the outcropping bedrock is applied, which is automatically transformed into a shear stress time history at the bottom of the mesh. As a consequence, the acceleration time-history at the base of the mesh is estimated as an output of the dynamic simulation and not as an a-priori evaluation [30]. Furthermore, boundaries simulating the free-field motion have been adopted at the right-hand and left-hand sides of the model.

Based on section 2, for any given study area and input motion, additional numerical analyses are required. Hence, for each considered input motion, on top of the 2D seismic ground response analysis for the slope of Fig. 2, another 2D analysis has been performed with the same mesh and boundary conditions, but where the ground consists solely of the bedrock material (V_R = 1250 m/s). In addition, various 1D seismic

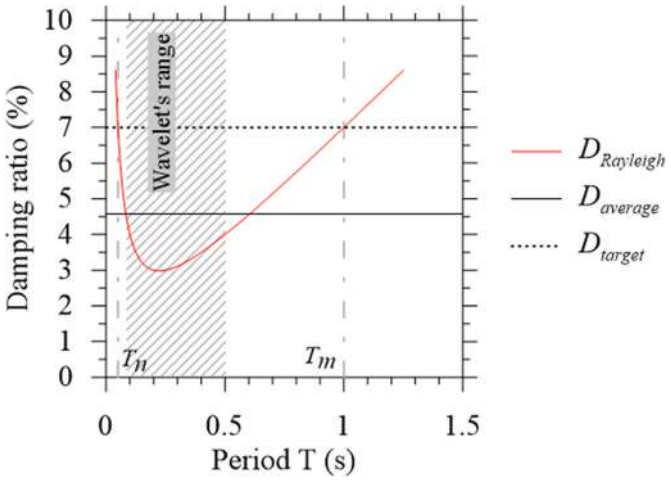

Fig. 4. Rayleigh damping implemented in the numerical analyses for both soil and bedrock layers.

ground response analyses are required to cover the whole study area. In this example, eight verticals have been selected to estimate the 1D seismic response, of which six (named V1 to V6) are placed at different locations within the slope (Fig. 2a) and two (named V_l and V_r) are located at the far end of both left and right sides of the 2D model, where free-field seismic response is expected. Each selected vertical of total height H_{TOT} is characterised by different thickness for both the soil H_S and the bedrock H_R layers (Table 2). The analyses of their seismic response have been also performed with the FE code, by simulating them as 2D ground columns of 1 m width. Tied-degree-of-freedom boundary conditions have been applied at the vertical sides, while the compliant base has been assigned to the bottom of each 1D ground column. It is reminded that for each 1D soil-bedrock column with the geometric characteristics of Table 2, another 1D ground column has also been analysed with the same total height H_{TOT}, but consisting solely of the bedrock material with V_R = 1250 m/s (see for example Fig. 1).

All the 2D and 1D dynamic analyses have been carried out under the assumption of fully undrained conditions. The standard Newmark solution method has been employed as time integration scheme during the dynamic stages, with Newmark parameters, α_N = 0.25 and β_N = 0.5, ensuring that the algorithm is unconditionally stable while being dissipative only at high frequencies [65].

4. Overall ground motion amplification

This section presents the numerical results from the 2D ground response analyses of the slope and the corresponding 1D ground response analyses for the eight selected locations of the verticals. Six sets of results are presented here, corresponding to the six input excitations. Results of interest are the spatially-variable peak ground acceleration at the ground surface of the 2D slope model, $a^S_{2D}(x)$, and the location-specific peak ground accelerations at the ground surface of the selected 1D soil-bedrock columns, $a^S_{1D}(x)$. Then, the amplification factors for both the 2D, $AF_{2D}(x)$, and the 1D, $AF_{1D}(x)$, models have been estimated for each input motion Wi (i = 1 to 6) and illustrated as a function of the distance x along the slope (Fig. 5). Lines of different

Table 2
Geometrical characteristics of the selected soil-bedrock columns.

	V_l	V1	V2	V3	V4	V5	V6	V_r
H_S (m)	55.5	50	50	51.3	50	51.7	50	42
H_R (m)	2.8	3.3	23.3	56.5	80.7	110.6	120.2	120.3
H_{TOT} (m)	58.3	53.3	73.3	107.8	130.7	162.3	170.2	162.3

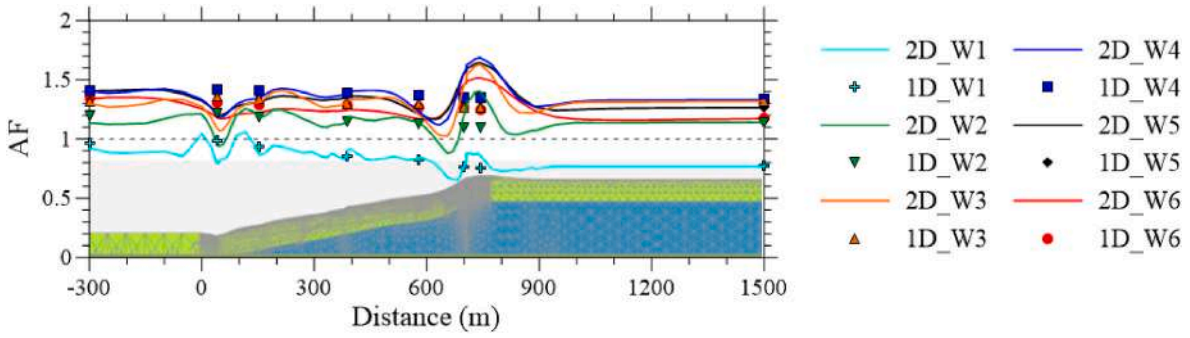

Fig. 5. Comparison between the spatially-variable 2D and location-specific 1D amplification factors along the slope for input motions with different frequency content.

colours depict $AF_{2D}(x)$ results for different input motions, while the symbols with the respective colours depict location-specific $AF_{1D}(x)$ results. Therefore, the vertical axis of the figure generically mentions AF, referring to both $AF_{2D}(x)$ and $AF_{1D}(x)$. The results in terms of $AF_{2D}(x)$ portray the total site amplification phenomenon along the slope, which includes topographic, stratigraphic and valley effects, while the results in terms of $AF_{1D}(x)$ depict locally the stratigraphic effects only. This direct comparison of the 2D to the 1D amplification gives a first indication about the slope portions affected by the topographic/valley effects. Indeed, it is evident that the non-horizontal ground surface profile is responsible for the amplification of the input motion around the upper portion of the slope (at the distance between 700 m and 800 m) and the de-amplification around the impluvium at the toe of the slope (at the distance between 0 m and 100 m) with respect to the 1D response. This trend is similar for all the input motions, irrespective of their frequency content. Instead, the 2D amplification profile tends to be equal to the 1D response far away from the sloping surface, where free-field seismic response is expected. A strong dependence of the amplitude of the amplification factors on the frequency content of the input motion is also clearly recognised. Indeed, an overall de-amplification of the motion at the ground surface is observed for the extremely short-period input motion (W1 in Fig. 5) since both the 1D and the 2D amplification factors achieve values smaller than 1.0 along the whole slope. Concurrently, as the predominant period of the input motion increases, the total amplification factors along the slope increase, achieving the maximum values when the slope is subjected to the long-period input motions (W4 and W5 in Fig. 5). On the other hand, when subjected to the motion with the longest predominant period, i.e. W6, the $AF_{2D}(x)$ profile is located between the low-period and the high-period motion response (Fig. 5). Another interesting feature is possibly the consistent reduction of the $AF_{2D}(x)$ curve between 600 m and 700 m, that could be related either to the topographic or to valley effects, but this clarification requires further decoupling of the amplification pattern.

5. Estimation of topographic effects

As described in section 2, the evaluation of the Topographic Amplification Factor $TAF(x)$ requires the estimation of the seismic response of a 2D homogeneous bedrock half-space model and of the corresponding 1D homogeneous bedrock columns at different locations along the slope, which are characterised by different total heights H_{TOT}. The 2D analysis provides the spatially-variable $a^R_{2D}(x)$, while the numerous 1D bedrock column analyses provide estimates of the location-specific $a^R_{1D}(x)$, which are used as the numerator and denominator of $TAF(x)$ in Eq. (3).

For the purpose of this example case, eight locations for 1D bedrock columns have been selected (Fig. 2). This means that the $TAF(x)$ may be exactly estimated only at these eight locations. To remedy this shortcoming without resorting to additional analyses, the results of the 1D simulations have been elaborated in terms of the ratio $AF^R_{1D}(x)$ of the maximum acceleration at the top of the 1D bedrock column $a^R_{1D}(x)$ to the maximum input acceleration a_0. The values of $AF^R_{1D}(x)$ have been correlated to the ratio of the stratigraphic period of the bedrock column $4H_{TOT}/V_R$ divided by the predominant period T_p of the input excitation. A linear variation of $AF^R_{1D}(x)$ with this ratio might be recognised in Fig. 6a, considering that in all cases the motion is de-amplified due to damping when passing through the bedrock material. This linear variation is fitted by Eq. (8):

$$AF^R_{1D} = \frac{a^R_{1D}}{a_0} = 1 - \alpha_1 \frac{4H_{TOT}}{V_R T_p} \tag{8}$$

where α_1 is a fitting parameter, assumed equal to 0.05 for the totality of the 1D bedrock column simulations, indicative of the amount of damping involved in the system.

To further validate this relation, additional 1D numerical simulations have been performed with reference to the same selected verticals along the slope, assigning the soil shear wave velocity, i.e. V_S, for the homogeneous half-space columns instead of V_R. These additional numerical results are also reported in Fig. 6a and this is why the seismic wave velocity value in the term appearing in the abscissa of this figure is $V_{R/S}$ and not V_S or V_R. Observe that these additional results also fall within the trend identified for the case of the bedrock homogenous half-space, generalising the applicability of the proposed formulation to any ground columns of different shear wave velocity. Essentially, Eq. (8) gives an indication of how much the maximum amplitude of the input motion should be expected to be de-amplified due to the height of the numerical model, whose increase introduces a greater amount of de-amplification due to damping. Theoretically, if a very small amount of damping ratio is employed (e.g., target damping ratio D_{target} of 0.01 %), no de-amplification of the input motion should be expected in the numerical simulations, but this would not be realistic for real case scenarios. It is worth noting that the numerical results are well captured by the analytical formulation for low values of the ratio $4H_{TOT}/(V_{R/S} \cdot T_p)$. However, for higher values of the above-mentioned ratio, the analytical formulation seems to slightly overpredict the response of the 1D bedrock columns subjected to the extremely short-period motion W1.

This is clearly shown by the one-to-one comparison of amplification factors AF^R_{1D}, as determined by empirical formulation and numerical simulations for all the cases in Fig. 6b, and the variation of the relative error R in estimating the AF^R_{1D} with the bedrock-excitation period-ratio, shown in Fig. 6c. It is noted that R is estimated as the difference between analytical and numerical predictions, normalised with respect to the latter. A satisfactory agreement between analytical and numerical estimates of AF^R_{1D} is observed, with the relative error R having an overall standard deviation of about 3 %. Thus, Eq. (8) may be adopted for predicting the maximum acceleration at the surface of 1D bedrock columns at any location, without having to perform the respective 1D

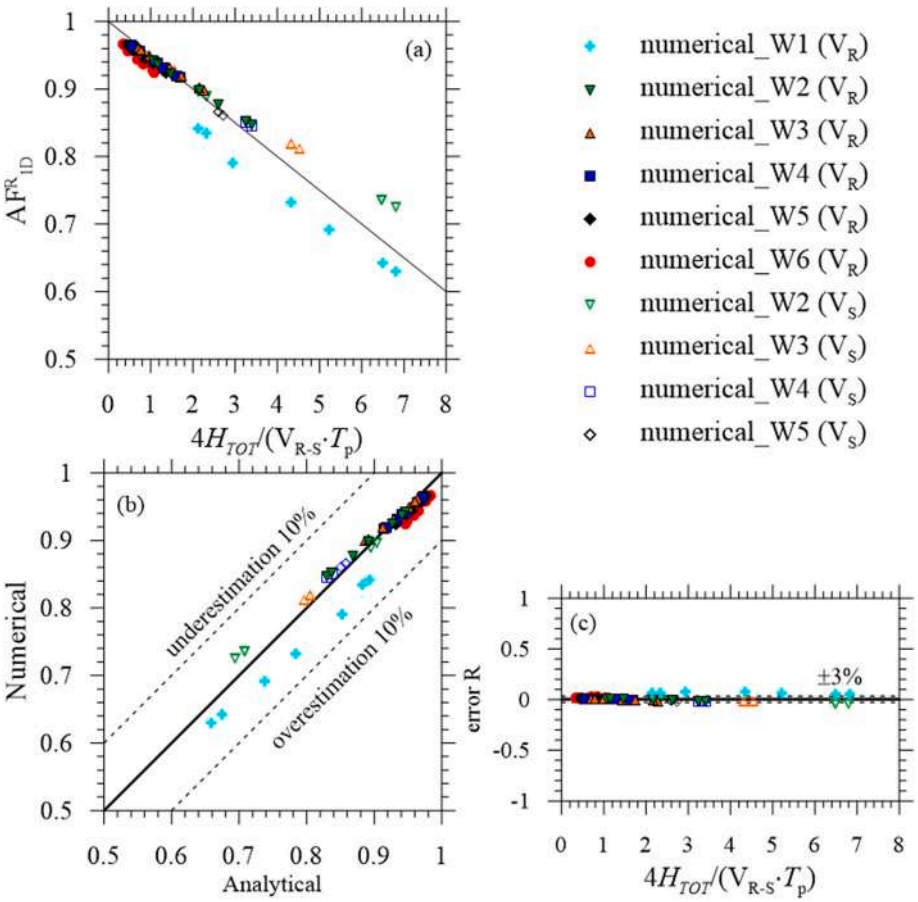

Fig. 6. (a) Variation of the AF^R_{1D} amplification factor with H_{TOT} for different input motions and different values of the shear wave velocity of the homogeneous column; (b) comparison between analytical and numerical estimates of the amplification factor AF^R_{1D}; (c) evaluation of the relative error in the analytical computation of the AF^R_{1D} amplification factor.

analyses. This is performed here for the study area, for which the 1D bedrock response is evaluated for all locations, characterised by increasing heights H_{TOT} from the toe to the crest of the slope.

The spatially-variable predictions of AF^R_{1D} obtained from Eq. (8) are reported in Fig. 7 together with the 1D numerical results in the locations of the verticals and show a good agreement for each input motion. The figure also includes the spatially-variable results from the 2D numerical simulation of the slope consisting of bedrock material in terms of the ratio a^R_{2D}/a_0, i.e., the ratio of the maximum acceleration predicted at the ground surface along the bedrock slope over the maximum input acceleration. These two curves do not coincide and give evidence to the distribution of the topographic effects along the slope for excitations with different frequency content. Indeed, by simply diving the two curves, one can estimate the Topographic Amplification Factor profile, $TAF(x)$, along the sloping surface, as per Eq. (3).

The computed 2D spatially-variable results in terms of $TAF(x)$ are compared in Fig. 8 for all six excitations. Observe that $TAF(x)$ is 1.0 for all input motions far from the sloping ground surface, where topographic effects are not expected. Regardless of the input motion characteristics, the highest topographic amplification concentrates around the crest of the slope and behind it, while de-amplification occurs around the toe of slope, where the topographic impluvium is located. These are typical results for homogeneous slopes (e.g., Ref. [53]). As expected, the excitation period of the input motion differently affects the distribution of the $TAF(x)$ profile. Indeed, long excitation periods, i.e. W4, W5 and W6 wavelets, provide smoother $TAF(x)$ profiles, for which the amplification factor is equal to 1.0 for most of the slope (specifically in the middle portion of the slope between 200 m and 600 m) and it increases up to about 1.3 approaching to the crest and decreases down to 0.9 approaching to the topographic impluvium. On the other hand, as the excitation period decreases (i.e. W1, W2 and W3 wavelets), the wavelength of the motion becomes smaller and thus more capable to capture the local irregularities of the slope topography. Accordingly, the $TAF(x)$ profiles appear to be rougher as the wavelet predominant periods decreases with values greater than one also in the middle portion of the slope. The lowest amplification factor due to topography around the toe, equal to about 0.8, is predicted for the lowest excitation period (i.e. W1).

Moreover, the distribution of $TAF(x)$, showing values lower than 1.0 between 600 m and 700 m, gives evidence to the reason for the reduction in the total amplification factor observed in Fig. 5, which is clearly related to the irregularity of the ground surface profile. This behaviour is more pronounced for input motions characterised by short excitation periods (e.g. W1, W2 and W3), while for long excitation periods (e.g. W4, W5 and W6) the surface topography plays a minor role in the seismic response of the slope at this specific location. It should be mentioned here that the above results are in good agreement with the literature for topography effects. For example, for the mild portion of the slope (distances 40–660 m) the relation of Bouckovalas and Papadimitriou [53] gives maximum topographic amplification of 1.05, while for the steep part of the slope (distances 660–720 m), the same analytical relation gives maximum topographic amplification that varies between 1.12 and 1.25, depending on the predominant period T_p of the motion. However, no study from the literature could provide the details of the spatial-variability of $TAF(x)$ depicted in Fig. 8.

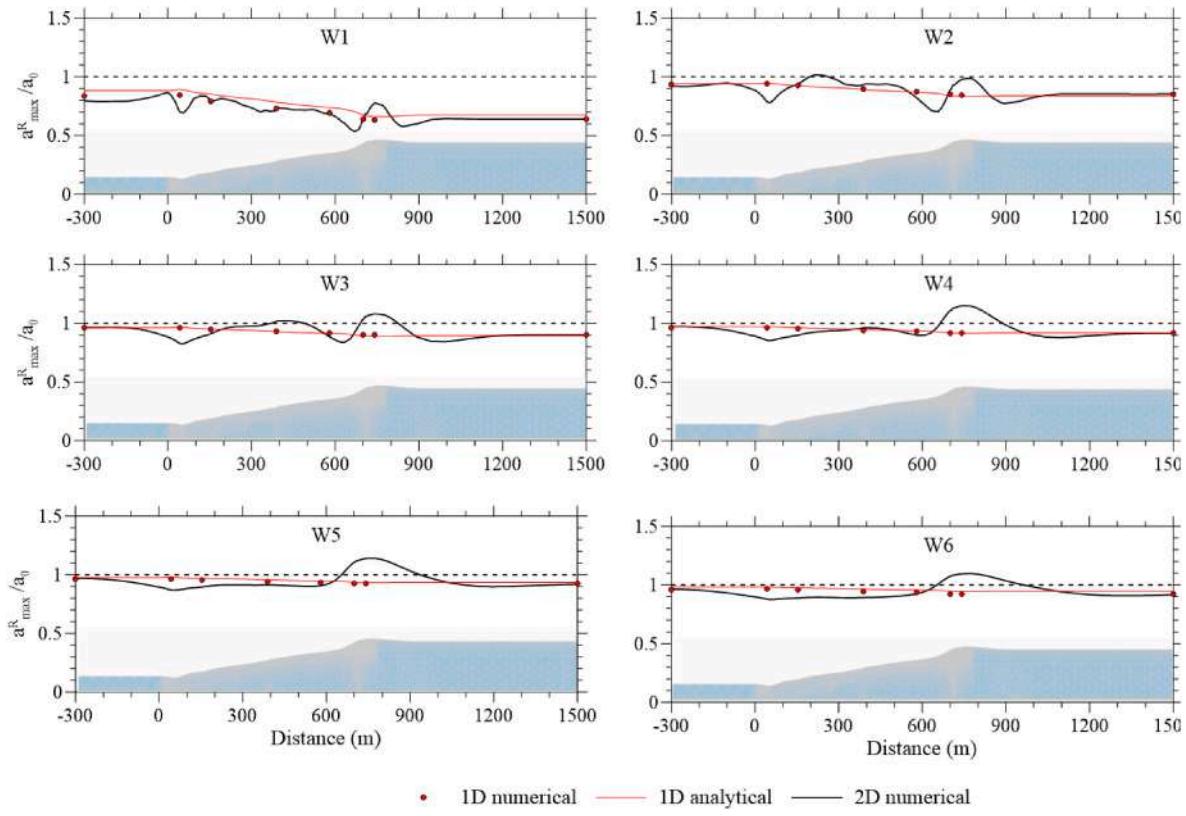

Fig. 7. Amplification of maximum acceleration along the ground surface for different input motions and homogeneous bedrock conditions (V_R = 1250 m/s) according to 2D and 1D ground response analyses and 1D analytical predictions.

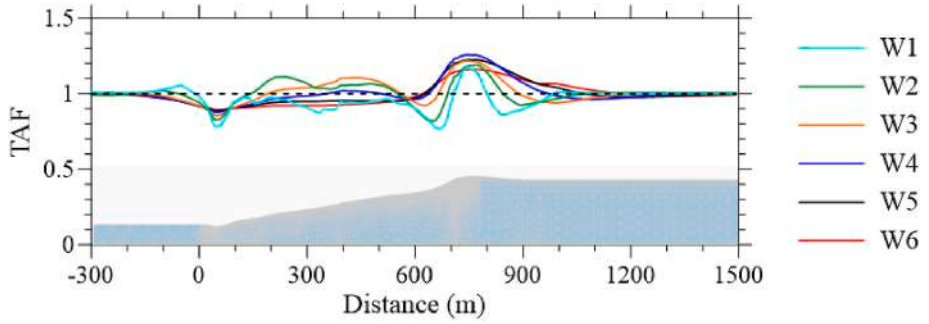

Fig. 8. $TAF(x)$ profile at ground surface for different input motions and homogeneous bedrock conditions (V_R = 1250 m/s).

6. Estimation of 1D stratigraphic effects

Ideally, the estimation of the 1D stratigraphic effects should be carried out by performing 1D numerical seismic ground response analyses for the soil-bedrock columns identified at the location of each observation point at the ground surface of the 2D slope model. Obviously, this requires the execution of numerous 1D analyses, implying high computational costs. Alternatively, empirical methods are also available in the literature, correlating the features of the seismic motions to site conditions, by means of a single soil parameter [72–76]. In the same line of thought, Bouckovalas and Papadimitriou [77] proposed a multi-variable relation for estimating the soil amplification factor of the maximum acceleration at the soil surface with respect to the maximum acceleration at the outcropping bedrock, on the basis of statistical analysis of a very large number of 1D equivalent-linear analyses for real sites and seismic recordings. This relation yields the amplification factor as a function of the normalised soil period, T_S/T_p, the peak acceleration at the outcropping bedrock, a_0, the bedrock-to-soil fundamental period ratio, T_R/T_S, and the number of equivalent cycles of harmonic excitation n. More specifically, the $T_S = 4H_S/V_S$ is the 1D fundamental period of the soil deposit of thickness H_S and $T_R = 4H_S/V_R$ is the 1D fundamental period of a layer of bedrock with the same thickness of the soil. Despite its merits in terms of computational cost in comparison to the numerous 1D analyses and in terms of accuracy in comparison to any of the empirical methods, this relation cannot be used here as it is developed for estimating the factor AF_{1D} of Eq. (1), since it only considers 1D soil columns of thickness H_S over bedrock and not soil-bedrock columns of total thickness $H_{TOT} = H_S + H_R$ (see Fig. 1).

To remedy this shortcoming, an attempt is made to modify the original relation of Bouckovalas and Papadimitriou [77], named B&P03 hereafter for brevity. The proposed modification is inspired by the results of the hereby performed 1D analyses for the eight selected verticals. The results of these analyses are collected in Fig. 9 in terms of the variation of the stratigraphic amplification factor AF_{1D} with the normalised soil period T_S/T_p. Firstly, these results show that the amplification factor takes its maximum value for $T_S/T_p = 1$ and, then, decreases

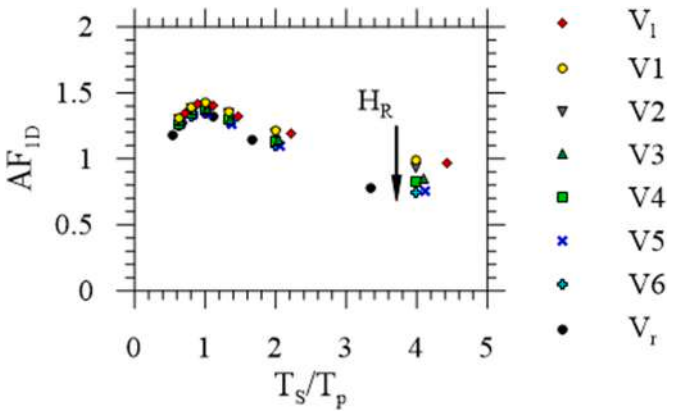

Fig. 9. Variation of the stratigraphic amplification factor AF_{1D} with the normalised soil period T_S/T_p from 1D numerical simulations of soil-bedrock columns.

in value with the increase of the normalised soil period $T_S/\ T_p$, as expected from the literature and as qualitatively captured by the B&P03 relation.

A closer look into these results reveals that for the same value of $T_S/\ T_p$, the AF_{1D} decreases for increasing thickness of the bedrock layer H_R included in the simulations (e.g., compare the seismic response of V1, V2, V4 and V6 verticals, characterised by the same H_S and different H_R). This secondary, but visible effect cannot be captured by the B&P03 relation and is the target of the proposed modification.

Specifically, based on this numerical evidence, the proposed modification introduces additional quantities accounting for the thickness of bedrock layer H_R. The final stratigraphic amplification factor AF_{1D} can be expressed by Eq. (9):

$$AF_{1D} = \frac{1 + \sqrt[4]{T_S/T_S^*}\,C_{1,a}\left(T_S/T_p\right)^2}{\sqrt{\left[1-\left(T_S/T_p\right)^2\right]^2 + \left(C_{2,a}^*\right)^2\sqrt[4]{T_S/T_S^*}\left(T_S/T_p\right)^2}} \tag{9}$$

where T_S^* is the 1D fundamental period of the soil-bedrock column of total height $H_{TOT} = H_S + H_R$. Observe that on the basis of Eq. (9), the amplification factor takes its maximum value for $T_S/T_p = 1$ and then decreases in value with an increase of the normalised soil period $T_S/\ T_p$, in qualitative accordance with what is expected in the literature and manifested by the simulation data shown in Fig. 9. The proposed modification of the B&P03 relation consists of the terms with an asterisk in Eq. (9), namely the added multiplier $\sqrt[4]{T_S/T_S^*}$ in the numerator and the denominator, as well as an alteration to the original $C_{2,a}$ term in the denominator (now denoted as $C_{2,a}^*$) that is explained below.

Specifically, for a soil-bedrock column of total height $H_{TOT} = H_S + H_R$, the equivalent shear wave velocity $V_{S,eq}^*$ based on the S wave travelling time can be estimated by Eq. (10):

$$V_{S,eq}^* = \frac{(H_S + H_R)}{\frac{H_S}{V_S} + \frac{H_R}{V_R}} \tag{10}$$

This $V_{S,eq}^*$ is used for the estimation of the 1D fundamental period T_S^* of the soil-bedrock column. Of interest is also the corresponding 1D fundamental period T_R^* of a layer of bedrock with the same thickness as the soil-bedrock column, given by Eq. (11):

$$T_R^* = \frac{4(H_S + H_R)}{V_R}$$
$$T_S^* = \frac{4(H_S + H_R)}{V_{S,eq}^*} \tag{11}$$

These two modified period values are used in the definition of the modified $C_{2,a}^*$, as given by Eq. (12):

$$C_{2,a}^* = d_{4,a} + d_{5,a}\frac{T_R^*}{T_S^*} \tag{12}$$

This term essentially accounts for the radiation damping effect on the amplification of the maximum acceleration, since the ratio of modified periods corresponds to the impedance ratio between $V_{S,eq}^*$ and V_R. The remaining terms of Eq. (9) are exactly as proposed in Bouckovalas and Papadimitriou [77], namely the coefficient $C_{1,a}$ is expressed as a function of the maximum acceleration of the outcropping motion a_0 and the number of equivalent cycles of harmonic excitation n, according to Eq. (13) and (14):

$$C_{1,a} = d_{1,a}\left(\frac{a_0}{g}\right)^{d_{2,a}} g(n) \tag{13}$$

with

$$g(n) = \frac{n^{d_{3,a}}}{1 + n^{d_{3,a}}} \tag{14}$$

Note that in the B&P03 relation, the effect of soil nonlinearity is introduced via an elongation of the soil period T_S entering the amplification factor (not considered here since the 2D response is considered visco-elastic) and via the increased hysteretic damping ratio, whose effect is introduced by the level of a_0 in Eq. (13) appearing in the numerator of Eq. (9). Specifically, given that the exponent $d_{2,a} < 0$ (see below), the higher the a_0, the greater the induced strain level and consequently the larger the hysteretic damping ratio, thus causing a decreased value of AF_{1D} in Eq. (9). Note also that the constants $d_{1,a}$, $d_{2,a}$, $d_{3,a}$, $d_{4,a}$ and $d_{5,a}$ in Eqs. (12)–(14) are fitting parameters, assumed equal to 1.20, −0.17, 0.50, 1.05 and 0.57, respectively, exactly as determined from a statistical analysis of a large number of available data by Bouckovalas and Papadimitriou [77]. Finally, note that if $H_R = 0$, then $T_S^* = T_S$, $T_R^* = T_R$ and the proposed Eq. (9) degenerates to the original relation of B&P03.

For each selected soil-bedrock column subjected to different excitations, the stratigraphic amplification factor has been evaluated through the proposed formulation, by assuming $a_0 = 0.02g$ (accounting for the low damping ratio of the visco-elastic analyses). The n is the number of cycles in the original B&P03 relation, but in its modified version proposed here it is essentially a fitting parameter that aids in attaining a good match of Eq. (9) with the numerical estimates of 1D stratigraphic amplification. Given that the waveform in all the input motions is qualitatively the same (see Fig. 3), a value of $n = 0.5$ was used for all Ricker wavelets. The values of significant entities entering Eq. (9) for each of the eight verticals (V_l, V1 – V6, V_r) and each of the six excitations (W1 – W6) are summarised in Table 3, on the basis of their geometrical properties reported in Table 2.

A first comparison between numerical and analytical estimates of the factor AF_{1D} is presented in Fig. 10, where the numerical data (symbols) are compared to the analytical curves obtained from Eq. (9) and the original B&P03 formulation. Each of the six subplots in this figure presents the comparison for a different vertical and all employed excitations. It can be observed that the numerical response is well captured by the proposed analytical relation for all verticals and for most of the input motions (i.e. W2 – W6 with predominant periods ranging from 0.16s to 0.5s). A slight overestimation is obtained in the prediction of the response of verticals excited by the extremely low-period wavelet W1 ($T_p = 0.08$s), corresponding to normalised soil periods T_S/T_p greater than 3.0. As expected, the B&P03 relation gives a good estimation of the factor AF_{1D} for those verticals characterised by very small thickness of the bedrock layer, e.g. V_l with $H_R = 2.8$ m (Fig. 10a) and V_1 with $H_R = 3.3$ m (not shown here for brevity), but its predictive ability worsens as the bedrock thickness H_R increases (Fig. 10b–f). This inaccuracy is resolved satisfactorily through the proposed modification.

A more complete comparison between the numerical predictions of the stratigraphic amplification factor AF_{1D} and its analytical estimates

Table 3
Characteristics of the selected vertical to be adopted in the proposed formulation (Eq. (9)).

	V_l	V1	V2	V3	V4	V5	V6	V_r
$V^*_{S,eq}$ (m/sec)	641.4	646.0	744.1	847.8	904.9	948.7	966.9	993.7
T_S (sec)	0.355	0.319	0.319	0.328	0.319	0.330	0.319	0.268
T_R (sec)	0.178	0.160	0.160	0.164	0.160	0.165	0.160	0.134
T^*_S (sec)	0.364	0.330	0.394	0.509	0.578	0.684	0.704	0.653
T^*_R (sec)	0.187	0.171	0.235	0.345	0.418	0.519	0.545	0.519
$T_S/\ T^*_S$	0.975	0.968	0.811	0.645	0.553	0.483	0.454	0.411

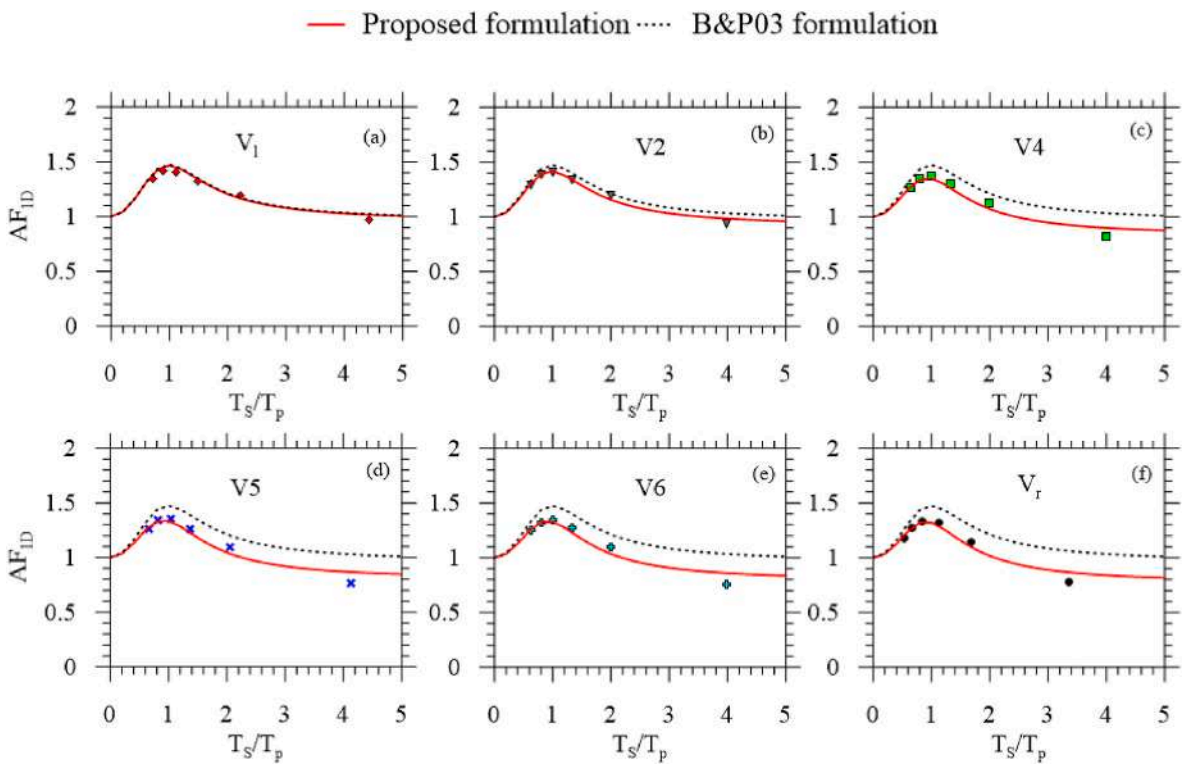

Fig. 10. Comparison between 1D numerical results for AF_{1D} and their analytical estimates as proposed by the literature relation B&P03 and its proposed modified version for a subset of available verticals and all seismic excitations.

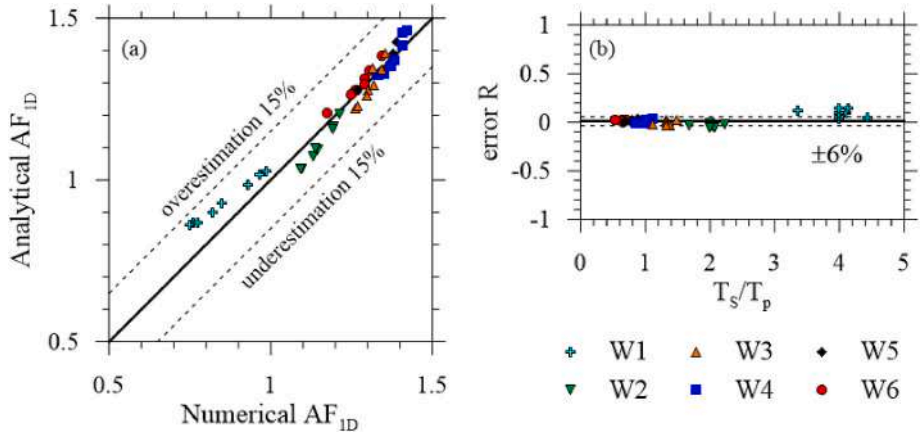

Fig. 11. (a) Comparison between analytical and numerical estimates of the amplification factor AF_{1D} for all verticals and excitations; (b) evaluation of the relative error in the analytical estimation of AF_{1D}.

obtained with the proposed Eq. (9) for all eight verticals and all six excitations is presented in Fig. 11. Specifically, Fig. 11a presents the one-to-one comparison between these estimates, while Fig. 11b presents the variation of the relative error R in the analytical estimation of the factor AF_{1D} as a function of the normalised soil period T_S/T_p. The comparison is very satisfactory without bias and a standard deviation of R of about 6 %, with the exception of the slight overestimation for the short-period motion (W1).

Having established the validity of the proposed formulation, the spatially-variable stratigraphic amplification factor $AF_{1D}(x)$ has been computed all along the 2D slope, on the basis of the H_S and H_R values for each location. Obviously, six different $AF_{1D}(x)$ have been computed, one for each excitation, considering the aforementioned selections for n and a_0.

The predictions are presented with differently coloured curves in Fig. 12, which also includes the results of 1D numerical estimates for all the verticals. The comparison is again quite satisfactory, except for the slight overestimation of the amplification for the extremely short-period motion (W1). The figure also gives a good example of how the proposed formulation may provide a reliable estimate of the stratigraphic amplification factor $AF_{1D}(x)$ with a very limited number of 1D ground response analyses (for verification purposes only). In terms of the actual results for the example slope, one may observe that the 1D stratigraphic amplification varies very slightly along the ground surface, as H_S is practically constant along the slope. On the other hand, this amplification varies significantly as a function of the frequency content of the applied excitation, as expected for stratigraphic effects. These results were qualitatively expected, since they are in tune with 1D wave propagation theory [67]. However, quantitative accuracy was achieved only after the proposed modification to the analytical formulation of Bouckovalas and Papadimitriou [77], which refers to including the bedrock section below the soil section in the 1D soil-bedrock columns.

7. Discussion

As described above, the total amplification factor $AF_{2D}(x)$ of the maximum horizontal acceleration along any slope surface may be approximately decoupled as the product of three spatially-variable independent amplification factors due to topographic, $TAF(x)$, stratigraphic, $AF_{1D}(x)$, and valley, $VAF(x)$, effects. What remains to be presented is the variation of the $VAF(x)$ factor along the slope, whose definition is given in Eq. (4). In practice, the $VAF(x)$ is essentially back-estimated on the basis of the numerically calculated $AF_{2D}(x)$ (see section 4) and the already estimated $TAF(x)$ and $AF_{1D}(x)$, according to the procedures described in sections 5 and 6, respectively.

Fig. 13 presents the back-estimated spatially-variable results in terms of $VAF(x)$ for all six excitations. Observe that $VAF(x)$ equals to 1.0 for all input motions near the edges of the model, since the bedrock does not outcrop and essentially 1D ground response conditions prevail. The only exception is the W1 motion, for which the $VAF(x) < 1.0$ at the right edge of the model, due to the pertinent over-prediction of $AF_{1D}(x)$ (see Fig. 12) that translates directly into an under-prediction of the $VAF(x)$ according to Eq. (4). More generally, the variation of this amplification factor is not so important in this example case, since its value oscillates around 1.0 ($\pm$0.3 at most) throughout the model and for all input excitations, and mostly upstream and downstream of the slope crest. In other words, since the example case does not include a closed soil valley (as shown, for instance, in the illustration of Fig. 1), valley effects are not important, in accordance to what was expected by the literature (e.g., Refs. [42–44]). However, it should be clarified that the exact pattern followed by the $VAF(x)$ profile all over the slope is greatly influenced by both the input motion characteristics and the morphology of the stratigraphic contact, this latter representing the only source of valley effects occurring in the example case.

Finally, the comparison of the total amplification factor $AF_{2D}(x)$ to the decoupled amplification factors, i.e. $TAF(x)$, $AF_{1D}(x)$ and $VAF(x)$ is reported in Fig. 14, separately for each of the different input motions. This comparison shows that, in the examined slope, stratigraphic effects are more pronounced than the topographic ones, while valley effects seem to be the least important. However, the peak total amplification near the crest of the slope is due primarily to topography effects with a small contribution due to valley effects. More generally, the highest total amplifications appearing for the long-period motions (W3, W4 and W5) may be safely attributed to the relatively higher stratigraphic effects due to 1D resonance of the soil layer of thickness $H_S \approx 50$ m with a $V_S = 626$ m/s over a much stiffer bedrock. As a whole, the decoupling procedure confirms what was expected for this example case. Indeed, it confirms that valley effects are generally unimportant for this case, but also that topographic effects are important and are most intense in the proximity of the highest slope inclination (between distances 660–720 m). Finally, as expected based on Fig. 2, stratigraphic effects are more or less uniform along the area, given the homogeneity and the approximately constant thickness of the soil layer, but in terms of intensity they depend significantly on the frequency of the input motion. However, quantitative conclusions regarding the spatially-variable importance of the three contributing amplification effects would have not been possible without the decoupling procedure proposed in this paper.

Finally, in order to bring the proposed procedure closer to engineering practice, it has been applied for the study of site effects of the same example slope when submitted to input motions that have the form of real earthquakes recordings. More specifically, the horizontal acceleration recordings of three seismic events have been employed as input motions, namely the Kozani, Gilroy and Aegion motions in Fig. 15a, b and c, respectively. In Fig. 15d, the corresponding elastic response spectra (for 5 % of critical damping) are also included and compared to the EC8 design spectrum for bedrock (Ground Type A). In comparison to the Ricker wavelets employed above, the real earthquake recordings are characterized by much longer duration, but their frequency content is within the same overall range (that is comparable with the range of the EC8 reference spectrum; see also Fig. 3). Specifically, the Kozani motion was recorded during the M6.5 Kozani-Grevena (Greece) earthquake in 1995 [78] and is characterised by a predominant period $T_p = 0.15$ s, while the Gilroy motion was recorded during the M5.9 Coyote Lake (USA) earthquake in 1979 [79] and is characterised by $T_p = 0.2$ s. The Aegion motion has a longer predominant period ($T_p = 0.43$ s) and was recorded during the M6.2 Aegion (Greece) earthquake in 1995 [13]. For

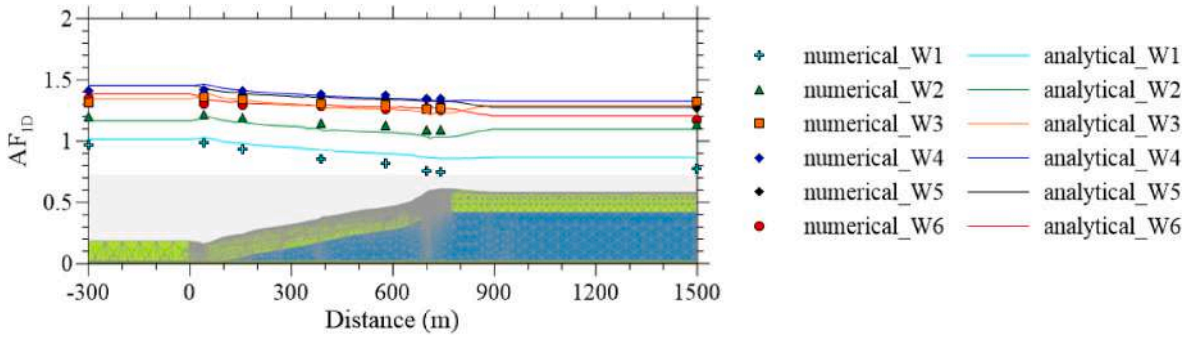

Fig. 12. Variation of 1D stratigraphic amplification factor AF_{1D} along the ground surface, on the basis of proposed formulation, and comparison to 1D ground response analyses for different input motions.

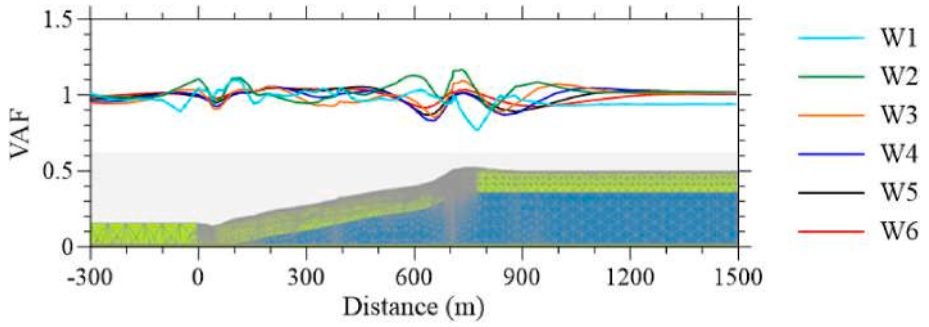

Fig. 13. VAF profiles at the ground surface of the example slope for different input motions.

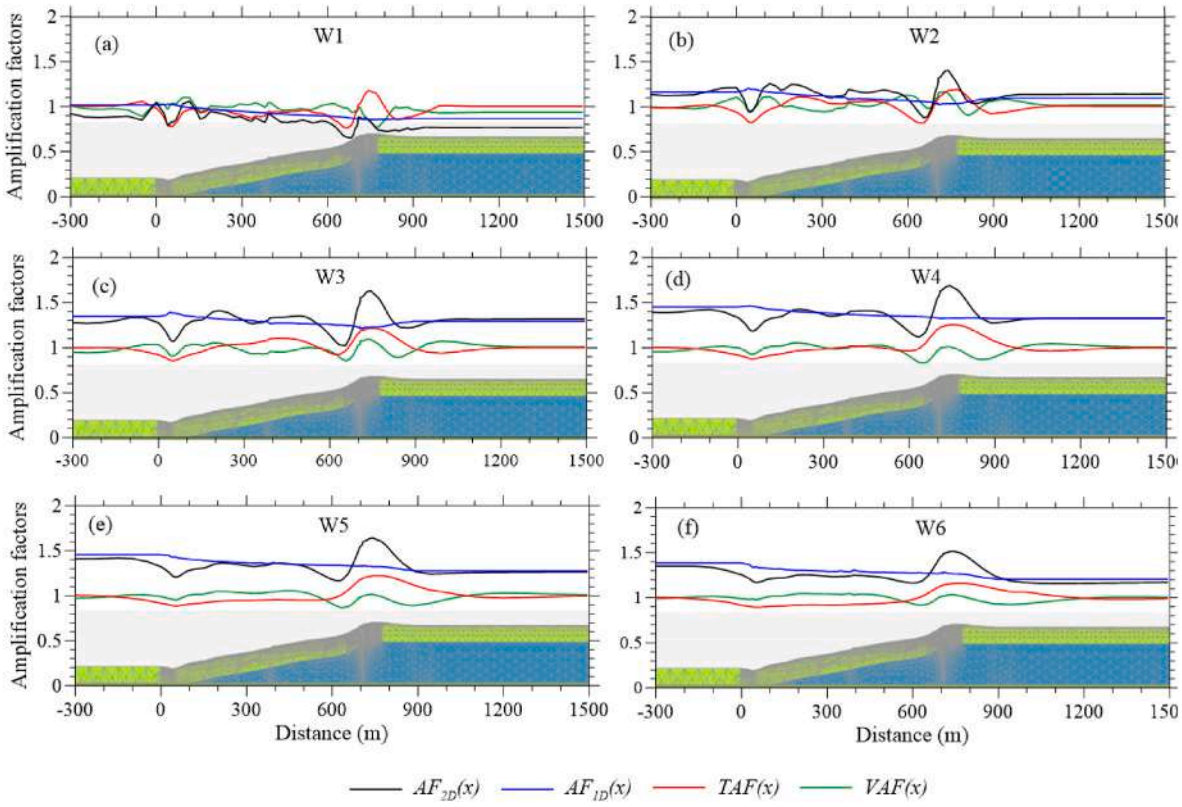

Fig. 14. Spatial variability of the decoupled amplification factors $TAF(x)$, $AF_{1D}(x)$ and $VAF(x)$, as compared to the total amplification factor $AF_{2D}(x)$, for different input motions.

the purpose of this application, the three input motions were filtered to 15 Hz, in order to satisfy the condition on the minimum element dimension of the FE mesh.

The results of the real earthquake simulations are illustrated in Fig. 16 in terms of the spatially-variable total amplification factor $AF_{2D}(x)$. Each subplot of this figure pertains to a different input motion and also includes the three corresponding spatially-variable independent amplification factors $TAF(x)$, $VAF(x)$ and $AF_{1D}(x)$ after their decoupling. Specifically, the stratigraphic amplification factor $AF_{1D}(x)$ has been evaluated assuming $a_0 = 0.02\,g$ in all cases and different values of n for the different input motions, selected in order to obtain the best fitting with the 1D numerical simulations of the soil-bedrock columns (also included with symbols in Fig. 16). Therefore, the n is assumed equal to 0.9 for both the Kozani and Gilroy motions, while it is set equal to 0.1 for the Aegion motion.

The hereby obtained amplification results are essentially in agreement with those predicted with the wavelet motions for the same slope. For example, observe that the almost uniform stratigraphic effects are more pronounced than the topographic ones, which become important near the crest (where the steepest surface inclination appears). On the other hand, again, the valley effects appear as the least important component of the overall amplification for this example case. Moreover, the spatial variability of the amplification factors is greatly influenced by the frequency content of the input motions, with the long period (Aegion) motion providing the smoothest profiles (Fig. 16c), as compared to the short period motions, i.e., the Kozani and Gilroy events (Fig. 16a and b). This is due to the wavelength of the travelling surface waves which is relatively smaller for the short period motions, in accordance with the literature (e.g., Ref. [53]). In closing, these additional simulations prove that the proposed procedure can be readily adopted for real earthquake recordings with sufficient accuracy, provided that the (clearly identified) predominant period T_p of the input motion is within the range of T_p of the wavelets used for its proposal.

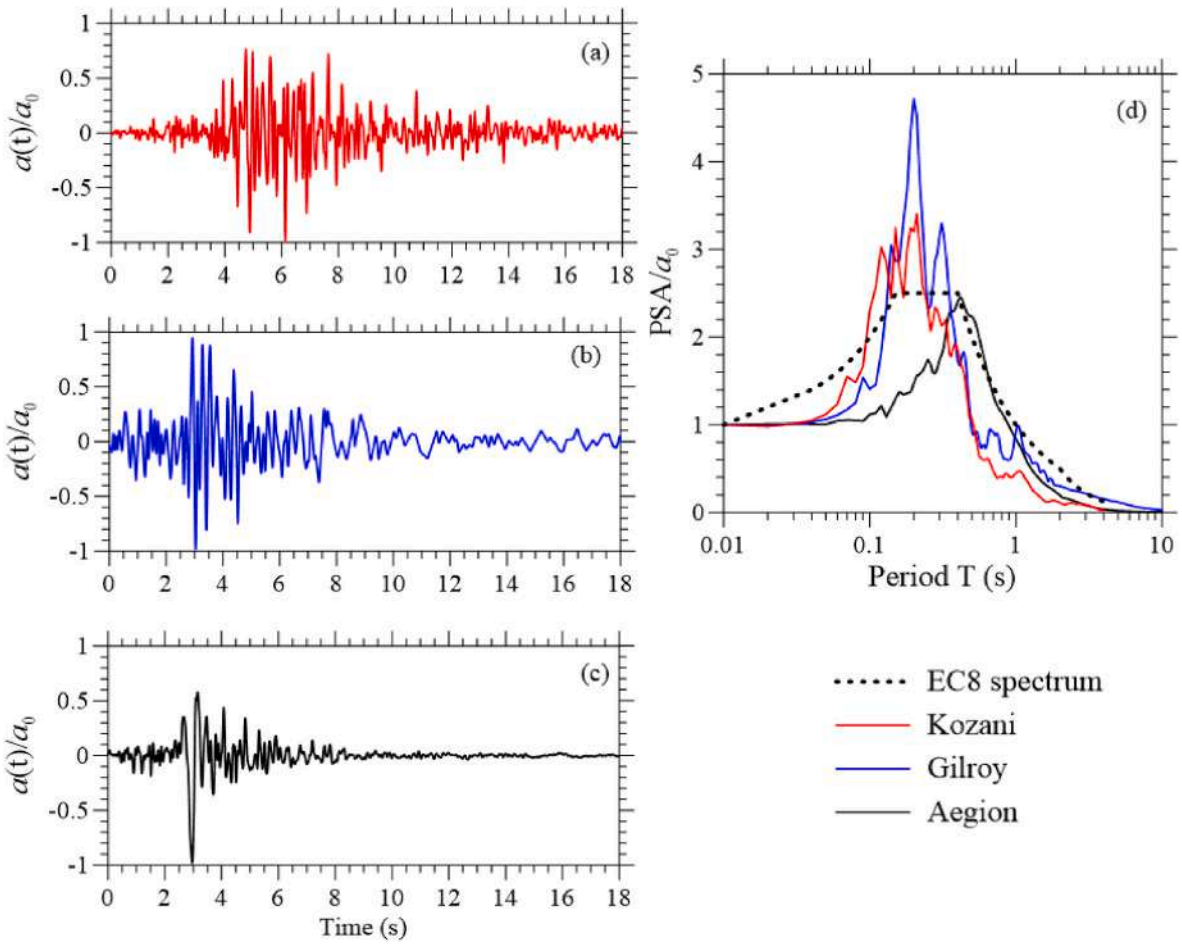

Fig. 15. Acceleration time histories of the (a) Kozani, (b) Gilroy and (c) Aegion earthquake motions and (d) corresponding elastic response spectra (for 5 % damping) compared to the EC8 design spectrum for bedrock (Ground Type A, for magnitudes M > 5.5).

8. Conclusions

This paper proposes an approximate procedure for decoupling the topographic, stratigraphic and valley effects involved in the 2D seismic amplification of the maximum horizontal acceleration at the ground surface of any area. The three homonymous amplification factors are spatially-variable and their multiplication yields the total amplification factor of this seismic intensity measure versus the maximum acceleration at outcropping bedrock for the area. For any given seismic excitation, the procedure requires the execution of two 2D ground response analyses, one for the actual site and another for the same site topography, but assuming that it entirely consists of bedrock material. Moreover, it requires the execution of a limited number of 1D ground response analyses for soil-bedrock and solely bedrock columns at different locations of the area, useful for the calibration and verification of a newly proposed analytical expression, based on the statistical analysis of 1D ground response analyses of real multi-layered soils proposed by Bouckovalas and Papadimitriou [77], which allows the estimation of the 1D amplification of the whole area. The alternative to the use of the analytical expression is to conduct 1D analyses for all locations along the area, which results in a high computational cost.

As any engineering methodology, the proposed procedure has drawbacks and limitations. An obvious limitation is that it only deals with the maximum horizontal acceleration and not any other seismic intensity measure. Nevertheless, the maximum horizontal acceleration is a crucial parameter for many civil engineering problems (e.g. slope stability, seismic demand of low-rise structures), hence its usefulness is self-evident. As future work, the proposed procedure could be similarly applied for other ground motion parameters, such as the whole of the acceleration response spectrum, or the acceleration spectrum intensity (ASI), which is another parameter for estimating site factors according to Eurocode 8 (EC8).

A second (but less significant) limitation is that this decoupling procedure can be applied, as proposed, only in cases that the same input (purely horizontal) acceleration time-history at the outcropping bedrock is valid throughout the study area (a very common assumption in most cases of engineering interest).

Another limitation concerns the reduced accuracy of this procedure for extremely low-period input motions (very high frequency content). However, such motions are rarely related to large magnitude events or have led to catastrophic consequences. More importantly, the procedure seems quite accurate for typically expected bedrock motions with predominant periods in the range of 0.16–0.5s, which comply with the typical range at least for the broader European area (see comparison with bedrock design spectrum of EC8 in Fig. 3b).

Moreover, the procedure is based on visco-elastic analyses and, hence, its accuracy should be verified when significant soil nonlinearity is expected (e.g. for high intensity motions). Secondly, it has been verified for the simple case of homogeneous soil over bedrock. Soil non-homogeneity may play a role in making the 1D amplification process more complicated. Nevertheless, the use of the modified analytical expression that was based on analyses of multi-layered soils [77] could aid in reducing the expected scatter in the results, without jeopardizing their overall accuracy, provided that all the soil layers are represented by an equivalent single layer characterized by average dynamic properties, in terms of shear wave velocity and damping ratio.

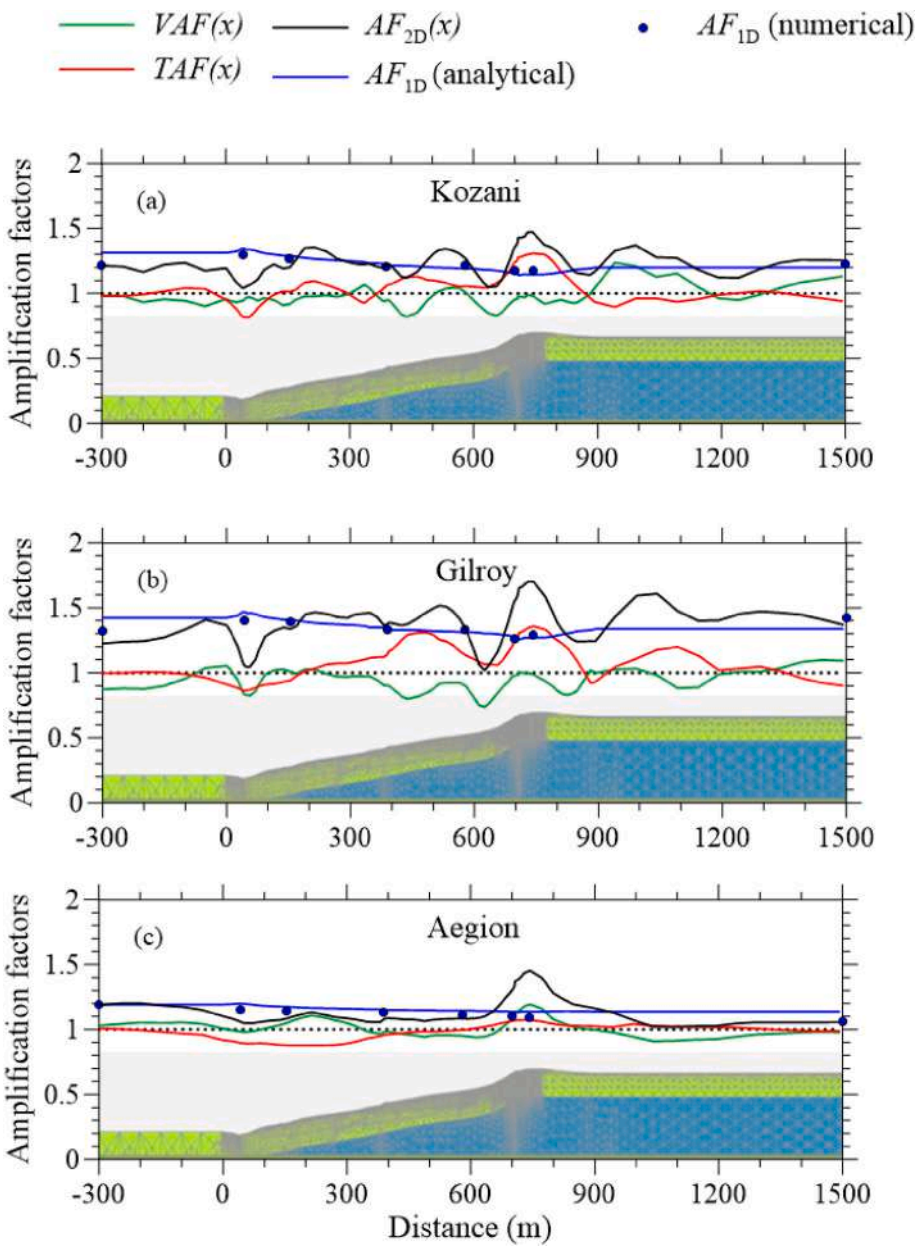

Fig. 16. Spatial variability of the decoupled amplification factors $TAF(x)$, $AF_{1D}(x)$ and $VAF(x)$, as compared to the total amplification factor $AF_{2D}(x)$, for different real earthquake recordings: (a) Kozani, (b) Gilroy and (c) Aegion motions.

In conclusion, despite its limitations, this paper describes a reliable tool for decoupling the topographic, stratigraphic and valley effects on the overall amplification of the maximum horizontal acceleration at the ground surface. Such decoupling is quite useful, since it allows the identification of regions within the study area that are mostly affected by each of these processes, thus guiding the need for additional site investigation or in-depth analysis. Moreover, it may prove useful for safer structural design since it aligns with the manner by which the seismic code provisions incorporate these effects on the definition of the design spectrum.

CRediT authorship contribution statement

Annamaria di Lernia: Writing – review & editing, Writing – original draft, Visualization, Validation, Methodology, Formal analysis, Data curation, Conceptualization. **Achilleas G. Papadimitriou:** Writing – review & editing, Writing – original draft, Visualization, Supervision, Methodology, Conceptualization. **Gaetano Elia:** Writing – review & editing, Supervision, Resources, Conceptualization, Methodology.

Declaration of competing interest

The authors declare that they have no known competing financial interests or personal relationships that could have appeared to influence the work reported in this paper.

Data availability

Data will be made available on request.

Acknowledgements

The research has been financially supported by the PON-AIM project (AIM1871082) and the PON-MITIGO project (ARS01_00964) fundings.

The third author is grateful for the financial support provided through the project “National Centre for HPC, Big Data and Quantum Computing – Spoke 5: Environment and Natural Disasters” (CN_00000013) funded by the National Recovery and Resilience Plan (PNRR). The funding provided by the Italian Ministerial grant PRIN 2022 PNRR “S.I.S.M.A.” (CUP_D53D23018050001) is also acknowledged.

References

[1] Bradley BA, Cubrinovski M. Near-source strong ground motions observed in the 22 february 2011 christchurch earthquake. Seismol Res Lett 2011;82:853–65. https://doi.org/10.1785/gssrl.82.6.853.
[2] Geli L, Bard PY, Jullien B. The effect of topography on earthquake ground motion: a review and new results. Bull Seismol Soc Am 1988;78:42–63. https://doi.org/10.1785/BSSA0780010042.
[3] Athanasopoulos GA, Pelekis PC, Leonidou EA. Effects of surface topography on seismic ground response in the Egion (Greece) 15 June 1995 earthquake. Soil Dynam Earthq Eng 1999;18:135–49.
[4] Fukushima Y, Irikura K, Uetake T, Matsumoto H. Characteristics of observed peak amplitude for strong ground motion from the 1995 hyogoken nanbu (kobe) earthquake. Bull Seismol Soc Am 2000;90:545–65. https://doi.org/10.1785/0119990066.
[5] Gazetas G, Kallou PV, Psarropoulos PN. Topography and soil effects in the MS 5.9 parnitha (Athens) earthquake: the case of adámes. Nat Hazards 2002;27:133–69. https://doi.org/10.1023/A:1019937106428.
[6] Biondi G, Maugeri M. Seismic response analysis of the Monte Po hill (Catania). In: Press W, editor. Seism. Prev. damage. A case study a Mediterr. City, Southampton, UK; 2005. p. 177–95.
[7] Assimaki D, Gazetas G, Kausel E. Effects of local soil conditions on the topographic aggravation of seismic motion: parametric investigation and recorded field evidence from the 1999 Athens earthquake. Bull Seismol Soc Am 2005;95:1059–89. https://doi.org/10.1785/0120040055.
[8] Gelagoti F, Kourkoulis R, Anastasopoulos I, Tazoh T, Gazetas G. Seismic wave propagation in a very soft alluvial valley: sensitivity to ground-motion details and soil nonlinearity, and generation of a parasitic vertical component. Bull Seismol Soc Am 2010;100:3035–54. https://doi.org/10.1785/0120100002.
[9] Cetin KO, Papadimitriou AG, Altun S, Pelekis P, Unutmaz B, Rovithis E, et al. The role of site effects on elevated seismic demands and corollary structural damage during the October 30, 2020, M7.0 Samos Island (Aegean Sea) Earthquake. Bull Earthq Eng 2022;20:7763–92. https://doi.org/10.1007/s10518-021-01265-z.
[10] Çelebi M. Topographical and geological amplification: case studies and engineering implications. Struct Saf 1991;10:199–217. https://doi.org/10.1016/0167-4730(91)90015-2.
[11] Çelebi M. Topographical and geological amplifications determined from strong-motion and aftershock records of the 3 March 1985 Chile earthquake. Bull Seismol Soc Am 1987;77:1147–67. https://doi.org/10.1785/BSSA0770041147.
[12] Kawase H, Aki K. Topography effect at the critical SV-wave incidence: possible explanation of damage pattern by the Whittier Narrows, California, earthquake of 1 October 1987. Bull Seismol Soc Am 1990;80:1–22. https://doi.org/10.1785/BSSA0800010001.
[13] Bouckovalas GD, Gazetas G, Papadimitriou AG. Geotechnical aspects of the 1995 Aegion, Greece earthquake. 2nd int. Conf. Earthq. Geotech. Eng., Lisbon, portugual. 1999. p. 739–48.
[14] Hough SE, Altidor JR, Anglade D, Given D, Janvier MG, Maharrey JZ, et al. Localized damage caused by topographic amplification during the 2010 M 7.0 Haiti earthquake. Nat Geosci 2010;3:778–82. https://doi.org/10.1038/ngeo988.
[15] Grelle G, Gargini E, Facciorusso J, Maresca R, Madiai C. Seismic site effects in the Red Zone of Amatrice hill detected via the mutual sustainment of experimental and computational approaches. Bull Earthq Eng 2020;18:1955–84. https://doi.org/10.1007/s10518-019-00777-z.
[16] Grelle G, Bonito L, Rosalba M, Iacurto S, Madiai C, Revellino P, et al. Topographic effects observed at Amatrice hill during the 2016–2017 Central Italy seismic sequence. Earthq Eng Eng Vib 2021;20:63–78. https://doi.org/10.1007/s11803-021-2005-z.
[17] Celebi M, Prince J, Dietel C, Onate M, Chavez G. The culprit in Mexico city—amplification of motions. Earthq Spectra 1987;3:315–28. https://doi.org/10.1193/1.1585431.
[18] Yegian MK, Ghahraman VG, Gazetas G. Seismological, soil and valley effects in kirovakan, 1988 Armenia earthquake. J Geotech Eng 1994;120:349–65. https://doi.org/10.1061/(ASCE)0733-9410(1994)120:2(349).
[19] Yegian MK, Ghahraman VG, Gazetas G. 1988 Armenia earthquake. I: seismological, geotechnical, and structural overview. J Geotech Eng 1994;120(1):1–20. https://doi.org/10.1061/(ASCE)0733-9410(1994)120:1.
[20] Graves RW. Modeling three-dimensional site response effects in the Marina District Basin, San Francisco, California. Bull Seismol Soc Am 1993;83:1042–63. https://doi.org/10.1785/BSSA0830041042.
[21] Lanzo G, Pagliaroli A. Numerical modeling of site effects at San Giuliano di Puglia (Southern Italy) during the 2002 molise seismic sequence. J Geotech Geoenviron Eng 2009;135:1295–313. https://doi.org/10.1061/(ASCE)GT.1943-5606.0000055.
[22] Castro RR, Pacor F, Puglia R, Ameri G, Letort J, Massa M, et al. The 2012 May 20 and 29, Emilia earthquakes (Northern Italy) and the main aftershocks: S-wave attenuation, acceleration source functions and site effects. Geophys J Int 2013;195:597–611. https://doi.org/10.1093/gji/ggt245.
[23] Cetin KO, Zarzour M, Cakir E, Tuna SC, Altun S. 2-D and 3-D basin site effects in Izmir-Bayrakli during the October 30, 2020 Mw7.0 Samos earthquake. Bull Earthq Eng 2023;21:5419–42. https://doi.org/10.1007/s10518-023-01738-3.
[24] Keefer DK. Landslides caused by earthquakes. GSA Bull 1984;95:406–21. https://doi.org/10.1130/0016-7606(1984)95.
[25] Sepúlveda SA, Murphy W, Jibson RW, Petley DN. Seismically induced rock slope failures resulting from topographic amplification of strong ground motions: the case of Pacoima Canyon, California. Eng Geol 2005;80:336–48. https://doi.org/10.1016/j.enggeo.2005.07.004.
[26] Yin Y, Wang F, Sun P. Landslide hazards triggered by the 2008 Wenchuan earthquake, Sichuan, China. Landslides 2009;6:139–52. https://doi.org/10.1007/s10346-009-0148-5.
[27] He J, Qi S, Wang Y, Saroglou C. Seismic response of the Lengzhuguan slope caused by topographic and geological effects. Eng Geol 2020;265. https://doi.org/10.1016/j.enggeo.2019.105431.
[28] Xu C, Shyu JBH, Xu XW. Landslides triggered by the 12 January 2010 Mw 7.0 Port-au-Prince, Haiti, earthquake: visual interpretation, inventory compiling and spatial distribution statistical analysis. Nat Hazards Earth Syst Sci Discuss 2014;2:1259–331. https://doi.org/10.5194/nhessd-2-1259-2014.
[29] Pignalosa A, Forte G, Budetta P, Santo A. Topographic amplification and debris remobilization as a cause for increasing rockfall hazard in seismic areas: a case study in Central Italy. Geomorphology 2022;403:108160. https://doi.org/10.1016/J.GEOMORPH.2022.108160.
[30] Falcone G, Boldini D, Amorosi A. Site response analysis of an urban area: a multi-dimensional and non-linear approach. Soil Dynam Earthq Eng 2018;109:33–45. https://doi.org/10.1016/j.soildyn.2018.02.026.
[31] Falcone G, Boldini D, Martelli L, Amorosi A. Quantifying local seismic amplification from regional charts and site specific numerical analyses: a case study. Bull Earthq Eng 2020;18:77–107. https://doi.org/10.1007/s10518-019-00719-9.
[32] di Lernia A, Buono C, Elia G. Evaluation of seismic site effects in a real slope through 2d fe numerical analyses. 9th Int. Conf. Comput. Methods Struct. Dyn. Earthq. Eng. - COMPDYN 2023, 2023:4110–24. https://doi.org/10.7712/120123.10705.20609.
[33] Gaudiosi I, Simionato M, Mancini M, Cavinato GP, Coltella M, Razzano R, et al. Evaluation of site effects at amatrice (central Italy) after the august 24th, 2016, mw 6.0 earthquake. Soil Dynam Earthq Eng 2021;144:106699. https://doi.org/10.1016/j.soildyn.2021.106699.
[34] Del Gaudio V, Wasowski J. Time probabilistic evaluation of seismically induced landslide hazard in Irpinia (Southern Italy). Soil Dynam Earthq Eng 2004;24:915–28. https://doi.org/10.1016/j.soildyn.2004.06.019.
[35] Del Gaudio V, Muscillo S, Wasowski J. What we can learn about slope response to earthquakes from ambient noise analysis: an overview. Eng Geol 2014;182:182–200. https://doi.org/10.1016/j.enggeo.2014.05.010.
[36] Pagliaroli A, Lanzo G, D'Elia B. Numerical evaluation of topographic effects at the nicastro ridge in southern Italy. J Earthq Eng 2011;15:404–32. https://doi.org/10.1080/13632469.2010.501892.
[37] Lanzo G, Silvestri F, Costanzo A, D'Onofrio A, Martelli L, Pagliaroli A, et al. Site response studies and seismic microzoning in the Middle Aterno valley (L'aquila, Central Italy). Bull Earthq Eng 2011;9:1417–42. https://doi.org/10.1007/s10518-011-9278-y.
[38] Papadimitriou A. An engineering perspective on topography and valley effects on seismic ground motion. In: Silvestri F, Moraci N, Antonielli S, editors. 7ICEGE. Rome: VII Int. Conf. Earthq. Geotech. Eng.; 2019.
[39] Bard P-Y, Bouchon M. The two-dimensional resonance of sediment-filled valleys. Bull Seismol Soc Am 1985;75:519–41. https://doi.org/10.1785/BSSA0750020519.
[40] Bard P-Y, Bouchon M. The seismic response of sediment-filled valleys. Part 1. The case of incident SH waves. Bull Seismol Soc Am 1980;70:1263–86. https://doi.org/10.1785/BSSA0700041263.
[41] Bard P-Y, Bouchon M. The seismic response of sediment-filled valleys. Part 2. The case of incident P and SV waves. Bull Seismol Soc Am 1980;70:1921–41. https://doi.org/10.1785/BSSA0700051921.
[42] Papadimitriou AG, Paraskevopoulos SA, Lamprakopoulos AN. Aggravation of spectral acceleration along 2D symmetrical trapezoidal valleys. Tessaloniki: 16th Eur. Conf. Earthq. Eng.; 2018.
[43] Vessia G, Russo S, Lo Presti DC. A new proposal for the evaluation of the amplification coefficient due to valley effects in the simplified local seismic response analyses. Ital Geotech J 2011;4:51–77.
[44] Riga E, Makra K, Pitilakis K. Aggravation factors for seismic response of sedimentary basins: a code-oriented parametric study. Soil Dynam Earthq Eng 2016;91:116–32. https://doi.org/10.1016/J.SOILDYN.2016.09.048.
[45] Psarropoulos PN, Tazoh T, Gazetas G, Apostolou M. Linear and nonlinear Valley Amplification effects on seismic ground motion. Soils Found 2007;47:857–71. https://doi.org/10.3208/sandf.47.857.
[46] Khanbabazadeh H, Iyisan R, Ansal A, Zulfikar C. Nonlinear dynamic behavior of the basins with 2D bedrock. Soil Dynam Earthq Eng 2018;107:108–15. https://doi.org/10.1016/j.soildyn.2018.01.011.
[47] Khanbabazadeh H, Hasal ME, Iyisan R. 2D seismic response of the Duzce Basin, Turkey. Soil Dynam Earthq Eng 2019;125:105754. https://doi.org/10.1016/j.soildyn.2019.105754.
[48] Khanbabazadeh H, Iyisan R, Ozaslan B. 2D seismic response of shallow sandy basins subjected to obliquely incident waves. Soil Dynam Earthq Eng 2022;153:107080. https://doi.org/10.1016/j.soildyn.2021.107080.

[49] Wong HL. Effect of surface topography on the diffraction of P, SV, and Rayleigh waves. Bull Seismol Soc Am 1982;72:1167–83. https://doi.org/10.1785/BSSA0720041167.
[50] Skiada E, Kontoe S, Stafford PJ, Potts DM. Canyon topography effects on ground motion. 16th world conf. Earthquake, 16WCEE, santiago, Chile. 2017.
[51] Solans D, Skiada E, Kontoe S, Potts DM. Canyon topography effects on ground motion: assessment of different soil stiffness profiles. Obras y Proy 2019;25:51–8.
[52] Zhang Z, Fleurisson J-A, Pellet F. The effects of slope topography on acceleration amplification and interaction between slope topography and seismic input motion. Soil Dynam Earthq Eng 2018;113:420–31. https://doi.org/10.1016/j.soildyn.2018.06.019.
[53] Bouckovalas GD, Papadimitriou AG. Numerical evaluation of slope topography effects on seismic ground motion. Soil Dynam Earthq Eng 2005;25:547–58. https://doi.org/10.1016/j.soildyn.2004.11.008.
[54] Tripe R, Kontoe S, Wong TKC. Slope topography effects on ground motion in the presence of deep soil layers. Soil Dynam Earthq Eng 2013;50:72–84. https://doi.org/10.1016/j.soildyn.2013.02.011.
[55] Régnier J, Bonilla L F, Bard P Y, Bertrand E, Hollender F, Kawase H, Sicilia D, Arduino P, Amorosi A, Asimaki D, Boldini D, Chen L, Chiaradonna A, DeMartin F, Ebrille M, Elgamal A, Falcone G, Foerster E, Foti S, Garini E, Gazetas G, Gélis C, Ghofrani A, Giannakou A, Gingery J R, Glinsky N, Harmon J, Hashash Y, Iai S, Jeremic B, Kramer S, Kontoe S, Kristek J, Lanzo G, Di Lernia A, Lopez-Caballero F, Marot M, McAllister G, Mercerat E D, Moczo P, Montoya-Noguera S, Musgrove M, Nieto-Ferro A, Pagliaroli A, Pisanò F, Richterova A, Sajana S, Santisi d'Avila M P, Shi Jian, Silvestri F, Taiebat M, Tropeano G, Verrucci L, Watanabe K. International benchmark on numerical simulations for 1D, nonlinear site response (PRENOLIN): verification phase based on canonical cases. Bull Seismol Soc Am 2016;106:2112–35.
[56] Régnier J, Bonilla L F, Bard P Y, Bertrand E, Hollender F, Kawase H, Sicilia D, Arduino P, Amorosi A, Asimaki D, Boldini D, Chen L, Chiaradonna A, DeMartin F, Elgamal A, Falcone G, Foerster E, Foti S, Garini E, Gazetas G, Gélis C, Ghofrani A, Giannakou A, Gingery J, Glinsky N, Harmon J, Hashash Y, Iai S, Kramer S, Kontoe S, Kristek J, Lanzo G, Di Lernia A, Lopez-Caballero F, Marot M, McAllister G, Mercerat E D, Moczo P, Montoya-Noguera S, Musgrove M, Nieto-Ferro A, Pagliaroli A, Passeri F, Richterova A, Sajana S, Santisi d'Avila M P, Shi J, Silvestri F, Taiebat M, Tropeano G, Vandeputte D, Verrucci L. PRENOLIN: international benchmark on 1D nonlinear site-response analysis—validation phase exercise. Bull Seismol Soc Am 2018;108:876–900. https://doi.org/10.1785/0120170210.
[57] Chiaradonna A. Defining the boundary conditions for seismic response analysis—a practical review of some widely-used codes. Geosciences 2022;12:83. https://doi.org/10.3390/geosciences12020083.
[58] Bardet JP, Tobita T. NERA: a computer program for nonlinearearthquake site response analyses of layered soil deposits. 2000.
[59] Lo Presti DC, Lai CG, Puci I. ONDA: computer code for nonlinear seismic response analyses of soil deposits. J Geotech Geoenviron Eng 2006;132:223–36. https://doi.org/10.1061/(ASCE)1090-0241(2006)132:2(223).
[60] Kottke AR, Rathje EM. Technical manual for strata 2013. 2013.
[61] Tropeano G, Chiaradonna A, D'Onofrio A, Silvestri F. An innovative computer code for 1D seismic response analysis including shear strength of soils. Geotechnique 2016;66:95–105. https://doi.org/10.1680/jgeot.SIP.15.P.017.
[62] Acunzo G, Falcone G, di Lernia A, Mori F, Mendicelli A, Naso G, et al. NC92Soil: a computer code for deterministic and stochastic 1D equivalent linear seismic site response analyses. Comput Geotech 2024;165:105857. https://doi.org/10.1016/j.compgeo.2023.105857.
[63] Kramer S, Stewart JP. Geotechnical aspects of seismic hazards. Earthq. Eng. From eng. Seismol. To performance-based eng. CRC Press; 2004. p. 107.
[64] Brinkgreve R, Kumarswamy S, Swolfs W. PLAXIS 2D connect edition V22.1. Reference manual; 2022.
[65] Amorosi A, Boldini D, Elia G. Parametric study on seismic ground response by finite element modelling. Comput Geotech 2010;37:515–28. https://doi.org/10.1016/j.compgeo.2010.02.005.
[66] Bathe KJ. Finite element procedures. second ed. Upper Saddle River, N.J.: Prentice Hall; 1996.
[67] Kramer S. Geotechnical earthquake engineering. Upper Saddle River, N.J.: Prentice Hall; 1996.
[68] Rayleigh J. The theory of sound. New York: Dover; 1945.
[69] Vucetic M, Dobry R. Effect of soil plasticity on cyclic response. J Geotech Eng 1991;117:89–107. https://doi.org/10.1061/(ASCE)0733-9410(1991)117:1. 89.
[70] Darendeli MB. Development of a new family of normalized modulus reduction and material damping curves. Austin: University of Texas; 2001.
[71] Joyner WB, Chen ATF. Calculation of non linear ground response in earthquake. Bull Seismol Soc Am 1975;65:1315–36.
[72] Ambraseys NN, Simpson KA, Bommer JJ. Prediction of horizontal response spectra in Europe. Earthq Eng Struct Dynam 1996;25:371–400. https://doi.org/10.1002/(SICI)1096-9845(199604)25:4<371::AID-EQE550>3.0.CO;2-A.
[73] Campbell KW. Empirical near-source attenuation relationships for horizontal and vertical components of peak ground acceleration, peak ground velocity, and pseudo-absolute acceleration response spectra. Seismol Res Lett 1997;68:154–79. https://doi.org/10.1785/gssrl.68.1.154.
[74] Borcherdt RD. Estimates of site-dependent response spectra for design (methodology and justification). Earthq Spectra 1994;10:617–53. https://doi.org/10.1193/1.1585791.
[75] Kawashima K, Aizawa K, Takahashi K. Attenuation of peak ground acceleration, velocity and displacement based on multiple regression analysis of Japanese strong motion records. Earthq Eng Struct Dynam 1986;14:199–215. https://doi.org/10.1002/eqe.4290140204.
[76] Spudich P, Joyner WB, Lindh AG, Boore DM, Margaris BM, Fletcher JB. SEA99: a revised ground motion prediction relation for use in extensional tectonic regimes. Bull Seismol Soc Am 1999;89:1156–70. https://doi.org/10.1785/BSSA0890051156.
[77] Bouckovalas GD, Papadimitriou AG. Multi-variable relations for soil effects on seismic ground motion. Earthq Eng Struct Dynam 2003;32:1867–96. https://doi.org/10.1002/EQE.306.
[78] Hatzfeld D, Karakostas V, Ziazia M, Selvaggi G, Leborgne S, Berge C, et al. The Kozani-Grevena (Greece) earthquake of 13 May 1995 revisited from a detailed seismological study. Bull Seismol Soc Am 1997;87:463–73. https://doi.org/10.1785/BSSA0870020463.
[79] Joyner WB, Warrick RE, Fumal TE. The effect of quaternary alluvium on strong ground motion in the Coyote Lake, California, earthquake of 1979. Bull Seismol Soc Am 1981;71:1333–49. https://doi.org/10.1785/BSSA0710041333.